UPPSALA
UNIVERSITET

Digital Comprehensive Summaries of Uppsala Dissertations from the Faculty of Science and Technology 2017

Linear models for multiscale materials simulations

Towards a seamless linking of electronic and atomistic models for complex metal oxides

AKSHAY KRISHNA AMMOTHUM KANDY

ACTA
UNIVERSITATIS
UPSALIENSIS
UPPSALA
2021

ISSN 1651-6214
ISBN 978-91-513-1141-8
urn:nbn:se:uu:diva-434283

Dissertation presented at Uppsala University to be publicly examined in Siegbahnsalen, Ångströmlaboratoriet, Lägerhyddsvägen 1, Uppsala, Wednesday, 24 March 2021 at 09:00 for the degree of Doctor of Philosophy. The examination will be conducted in English. Faculty examiner: Senior Lecturer Ben Hourahine (University of Strathclyde, Department of Physics).

Abstract

Ammothum Kandy, A. K. 2021. Linear models for multiscale materials simulations. Towards a seamless linking of electronic and atomistic models for complex metal oxides. *Digital Comprehensive Summaries of Uppsala Dissertations from the Faculty of Science and Technology* 2017. 62 pp. Uppsala: Acta Universitatis Upsaliensis. ISBN 978-91-513-1141-8.

Multiscale modelling approaches, connecting data from electronic structure calculations all the way towards engineering continuum models, have become an important ingredient in modern materials science. Materials modelling in a broader sense is already amply used to address complex chemical problems in academic science, but also in many industrial sectors. As far as multiscale modelling is concerned, however, many challenges remain, in particular when it comes to coupling and linking the various levels along the multiscale ladder in a seamless and efficient fashion.

This thesis focusses on the development of new and efficient linear models to improve the quality and parameterisation processes of the two-body potentials used in empirical and semi-empirical methods within a multiscale materials modelling framework. In this regard, a machinery called curvature constrained splines (CCS) based on cubic splines to approximate general two-body potentials has been developed. The method is linear, and parameters can be easily solved in a least-square sense using a quadratic programming approach. Moreover, the objective function is convex, implying that global minima can be readily found. This makes the optimisation process easy to handle and requires little to no human effort. Initial tests to validate the method were performed on molecular and bulk neon systems. Later, the method was extended to incorporate long-range interactions by including atomic charges. The capability of the method was demonstrated for ZnO polymorphs, and at the same time benchmarked towards the conventional Buckingham potentials applied to the same problem. The results indicate that the CCS+Q method performs on par with the Buckingham approach, but is much faster and easier to parameterise. The merits of the method is further demonstrated with an exploration of size and shape dependent stability of CeO_2 nanoparticles.

Having established the framework of the CCS methodology, the method was further used to develop repulsive potentials for the semi-empirical self-consistent charge density functional tight binding (SCC-DFTB) method. The generation of the repulsive potentials is normally a tedious and time-consuming task. The CCS methodology makes this process significantly more efficient, and further provides new opportunities to explore the limits of the SCC-DFTB method. The development of repulsive potentials for bulk Si polymorphs showed that it is possible to retrieve a good description of each individual polymorph, but impossible to obtain an acceptable joint description of all polymorphs. The results indicated that a transferable repulsive potential needs to have coordination dependence, and by the use of a many-body artificial neural network representation for the repulsive potential, it was indeed possible to obtain a global transferability. The CCS methodology was finally used to model a system of considerable chemical diversity and complexity, namely reduced CeO_2 within the SCC-DFTB formalism. Here, the CCS framework facilitated the development of an efficient workflow that yielded a harmonized description of Ce ions in different oxidation states. In short, the introduced CCS-based workflow proved to extend the applicability of SCC-DFTB to complex oxide systems with correlated electronic states.

To conclude, the CCS methodology is demonstrated to be a versatile tool for efficient linking between (and within) electronic and atomistic models.

Keywords: Force fields, Electronic structure calculations, CCS, DFTB, CCS+Q, repulsive fitting

Akshay Krishna Ammothum Kandy, Department of Chemistry - Ångström Laboratory, Structural Chemistry, Box 538, Uppsala University, SE-751 21 Uppsala, Sweden.

ISSN 1651-6214
ISBN 978-91-513-1141-8
urn:nbn:se:uu:diva-434283 (http://urn.kb.se/resolve?urn=urn:nbn:se:uu:diva-434283)

Dedicated to my wife and parents

List of papers

This thesis is based on the following papers, which are referred to in the text by their Roman numerals.

I **CCS: A software framework to generate two-body potentials using Curvature Constrained Splines**
Akshay Krishna Ammothum Kandy, Eddie Wadbro, Christof Köhler, Pavlin Mitev, Peter Broqvist, and Jolla Kullgren
Computer Physics Communications, **258**, 107602. (2020)

II **Development of efficient linearly parameterized force fields for ionic materials**
Akshay Krishna Ammothum Kandy, Eddie Wadbro, Peter Broqvist, and Jolla Kullgren
In Manuscript

III **Curvature constrained splines for DFTB repulsive potential parameterization**
Akshay Krishna Ammothum Kandy, Eddie Wadbro, Balint Aradi, Peter Broqvist, and Jolla Kullgren
Journal of Chemical Theory and Computation (Accepted)

IV **Accurate description of Ce 4f states in reduced ceria using SCC-DFTB+U simulations**
Bojana Kocmaruk, Akshay Krishna Ammothum Kandy, Jolla Kullgren, and Peter Broqvist
In Manuscript

Author Contribution

Paper I: I developed the CCS method along with the co-authors. I wrote the python package, performed the test calculations, analyzed the data and wrote the first draft of the paper.

Paper II: I planned the work with the co-authors and extended the CCS method. I wrote the python calculator for the method, optimised the potentials, and performed most of the calculations. I wrote the first draft of the paper

Paper III: I was involved in major part of planning, development and execution of this project. I performed the calculations and analyzed the results with the help from the co-authors and wrote the first draft of the paper.

Paper IV: I was involved in major part of the planning, discussion, and analysis of the results in this work. I contributed to the development and testing of the CCS repulsive potentials used in this project.

Contents

1. Introduction

1.1 Materials chemistry

Materials science is an interdisciplinary endeavor that requires domain-specific knowledge from chemistry, physics, and engineering. The field of materials engineering focuses mainly on the production and application of materials. The areas of materials chemistry and physics, on the other hand, often follow the atomic hypothesis[1] in its view on matter. Their aim is to gain a fundamental understanding on how the atomic (or electronic) structure determines the chemical and physical properties of a material. Materials chemistry forms a scientific foundation to design, synthesize, characterize, and understand existing and new functional materials.

Materials are truly multiscale in nature, i.e., their properties are governed by events occurring at various time and length scales. While the functionality of many materials is dictated by the well-defined bulk properties such as electronic band gaps, elastic modulus, dielectric constants, etc., there are many situations where functionality stems from the deviations from the bulk behavior. For example, the electronic and optical properties of nanomaterials have shape and size dependency, in contrast to bulk[2,3].

An exciting class of materials is the reducible metal oxides that have attracted considerable research interest due to their versatile chemistry and a wide variety of applicability, e.g. within heterogeneous catalysis[4], energy storage[5], fuel cells[6], and batteries[7], to name a few. The versatility and rich chemistry of reducible metal oxides are often ascribed to their low oxygen-defect-formation energies and multiple metal ion oxidation states[8,9]. To fully comprehend the complex chemistry of reducible oxides detailed knowledge about the electronic structure, the shapes of nanoparticles, the locations of metal ions, the interactions (long-range) of defects, and their interplay is required. For example, in the case of ceria nanoparticles, the locations of Ce^{3+} ions formed upon reduction and the relative stability of surface and subsurface defects in ceria are yet to be fully elucidated. Unfortunately, experimental techniques are often too obtuse and cannot alone provide a holistic atomic-level description; they need to be complemented with theoretical modelling.

1.2 Modelling in materials chemistry

In the past decades, computational modeling has become a powerful tool for identifying new materials and tailoring properties to improve applications. The rapid advancement of computing power, algorithms and softwares is beginning to link understanding at the microscopic level to functional behavior at the macroscale. However, real-world phenomena are often highly complex with a large number of degrees of freedom and span a wide range of length- and time-scales. Computational models are yet to encompass such phenomena in full detail. Inevitably, we approximate models by coarse-graining the degrees of freedom based on different interactions, that depend on magnitudes of length- and time-scales. This has led to the development of the sequential multiscale ladder shown in Fig. 1.1, which forms the backbone of modern-day computational material science. Multiscale modelling methods have been successfully used in a variety of applications, including heterogeneous catalysis[10], batteries,[11,12] and memory devices[13], to name a few.

Traditionally, multiscale models are classified according to time- and length-scales. However, with the rapid development in computational power, the boundaries between the scales have become ill-defined. This thesis follows the ontology suggested by the European Materials Modelling Council (EMMC) to bring forth a homogenized vocabulary among researchers working at various levels of multiscale modelling, both in academia and industry. According to Ref. 14, models are defined as a combination of physics equations (PE) and materials relations (MR). The physics equations and the materials relations for a particular problem are formulated in terms of one of four entities: electrons, atoms, mesoscopic particles, or continuum. The physics equations and the materials relations together constitute "the governing equations" or "the model", and describe the behaviour of the entity in focus (electrons, atoms, ...). Within the EMMC framework, the models used in materials modelling are thus classified based on the four entities. Strictly, by the above definitions, the hierarchy of models should be called "multi-equation-modelling" rather than "multiscale" modelling. In the rest of the thesis, multiscale modelling refers to multi-equation-modelling.

Electronic models form the lowest level in the multiscale hierarchy, where electrons are the entity and the Schrödinger equation is the physics equation. Calculations at the electronic level provide information about the electronic structure and structural properties (lattice parameter, elastic constants, etc.). The subsequent *atomistic models* have atoms as the entity and the physics equation follow Newtonian mechanics. Atomistic models typically provide information about the structural and dynamical properties of a system. Next are the *mesoscopic models* where nanoparticles, grains, or beads (a group of molecules/atoms) are the entities,

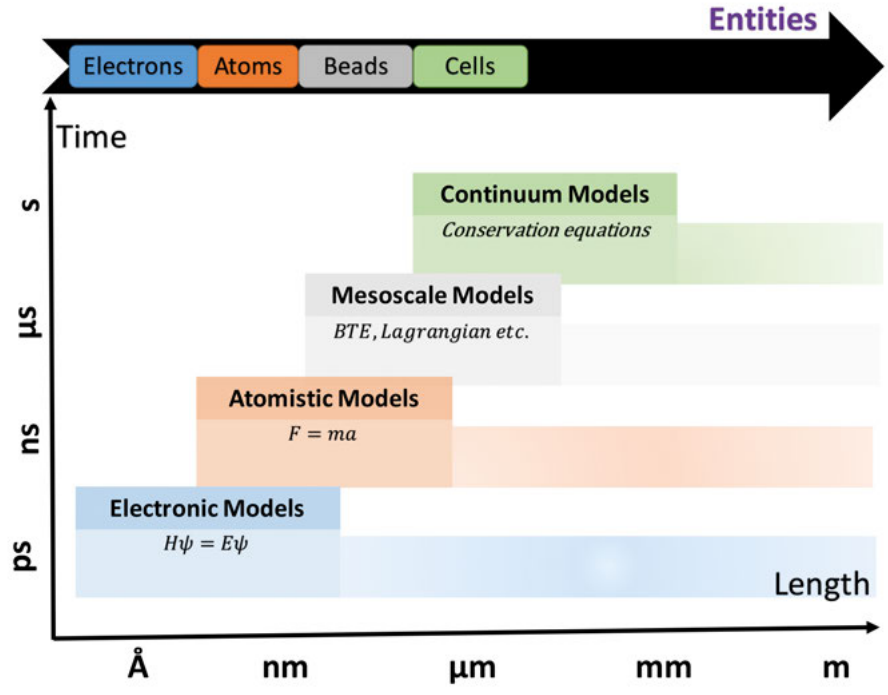

Figure 1.1. A schematic overview of the multiscale hierarchy. Models are arranged according to their characteristic length- and time-scales. The entities and their physics equations are also listed.

and Boltzmann transport equations (BTE), Newtonian mechanics, etc., are the physics equations. Mesoscopic models provide mainly details about morphology, thermal stability, domain formation. The last step is the *continuum models*, where finite volumes or cells are the entities, and the physics equations are conservation laws. Continuum simulations are used, for example, to predict crack propagation, or, the macroscopic structural behavior of a material. In principle, the microscopic origin of any macroscopic phenomenon could be studied by coupling and linking a multitude of models in the multiscale hierarchy. The coupling and linking of models refer to the integration of different models into a single workflow such that the output from one is used as input to the other (linking) and vice-versa (coupling). In this context, a workflow describes how the models are arranged into a chain. A bottleneck often encountered in many multiscale simulation workflows is the transfer of information from one model to the other. In this regard, complex mathematical functions are often used, e.g. force fields in the linking of the electronic and atomistic levels. At these levels, the currently available linking methods can be classified into two types: *i)* physics-based methods and *ii)* data-driven methods. A recent recent trend among com-

putational chemists is to develop purely data-driven methods with less emphasis on the chemical nature of the problem. These approaches have been quite successful but are often very cumbersome to use in practice. In my view, the data-driven methods will be extensively used for *coupling and linking* different models in the future. The question to address is — How to retain the "chemical intuition" in data-driven methods in a reliable and computationally efficient manner compared to physics-based methods?

1.3 Scope of the thesis

This thesis summarizes my efforts to develop, understand and apply new methods/schemes that are useful to fill some "gaps" in the multiscale modelling approach. The primary focus lies on linking the electronic and atomistic models (see Fig. 1.1). The methods developed in this thesis comprise an initial step to improve data-driven methods taking inspiration from physics-based methods. Fig. 1.2 provides an overview of the thesis showing the relation between the various methods and the corresponding papers.

In **Paper I**, the Curvature Constrained Splines (CCS) method was developed to facilitate an efficient construction of two-body potentials. The CCS method was used to construct simple, effective two-body potentials from ab initio data for neon. The method was also packaged into a python package, which is freely available at `https://github.com/aksam432/CCS`. **Paper II** presents an extension to the CCS method called CCS+Q, where long-ranged electrostatics are included for modelling ionic materials. We show that the short-ranged potential and long-ranged electrostatics can be optimised simultaneously using quadratic programming (QP). The method is validated using bulk ZnO and CeO_2 nanoparticles as examples.

In **Paper III** and **Paper IV**, the CCS method was further used to link models within the electronic level. In **Paper III**, the CCS methodology was used to improve aspects of the self-consistent charge density functional tight binding (SCC-DFTB) method. Owing to the unique properties of the CCS formalism, also questions regarding the transferability of the SCC-DFTB method could be addressed. It was shown that the transferability of the method is limited when using a two-body repulsive potential. If instead a many-body artificial neural network (ANN) representation is used as repulsive potential, the transferability was shown to be significantly improved. In **Paper IV**, a workflow utilising a "f in-core" approach to study electron localisation in strongly correlated reducible metal oxide systems within the SCC-DFTB formalism was in-

troduced and validated. In this workflow, the CCS methodology is key to harmonize the treatment of Ce ions in different oxidation states.

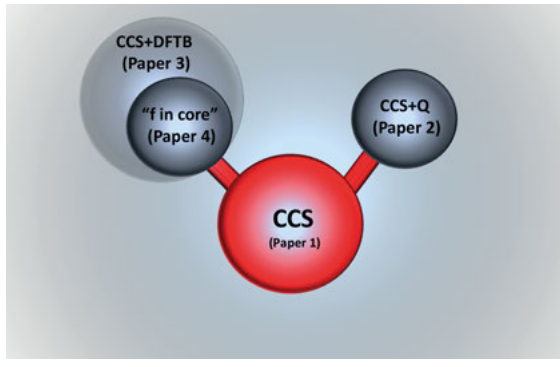

Figure 1.2. An overall sketch of the thesis content showing the relations between the various methods developed. The CCS development follows two branches. The first one (to the right) comprises an electronic to atomistic linking through the generation of the CCS+Q model based on QM data. The second branch (left) refers to linking within the electronic level. Here, the CCS methodology is used as the repulsive potential within the SCC-DFTB method to reproduce ab initio reference data.

2. Theory and methods

In this chapter, I will give the theoretical background for the scientific models and the main mathematical methods used in this thesis. The intention is not to give a complete overview, but instead focus on key concepts and equations needed to understand the scope of this thesis. I will follow the ontology introduced in the introduction for the multi-scale modelling approach, but here solely focus on the electronic and atomic levels, and the mathematics behind the *"coupling and linking"* between them.

2.1 The multiscale modelling approach

Quantum mechanical (QM) methods form the lowest rung in the multi-scale hierarchy, cf. Fig. 1.1. At this level, describing electrons, the Schrödinger equation is the key to understand the time evolution and properties of a system. However, the Schrödinger equation is only solvable for a few simple problems. So, approximations are necessary for any practical use. One such approximation is the Born-Oppenheimer (BO) approximation, which states that the motion of electrons can be decoupled from the motion of the atomic nuclei. Equipped with the BO approximation, we can describe the potential energy surface (PES) as a function of atomic nuclei positions.

In QM methods, electronic Hamiltonians are used to evaluate the PES. The most popular methods to construct the electronic Hamiltonian include the wave-function based Hartree-Fock (HF)[15] method or the Density Functional Theory (DFT)[16,17]. Both the HF method and DFT has many limitations. HF, for example, lack electron correlation, and DFT has problems with electron self-interaction and cannot describe dispersion interactions, both resulting in major problems for certain systems. Though post-HF methods[18] account for correlation effects, and novel advanced DFT functionals include effects of non-local Fock exchange and non-local correlation, which resolves many issues, these methods often become too computationally costly for studies of large systems and long time scales.

Within the framework of QM models, semi-empirical methods can overcome the computational cost posed by DFT/HF methods[19]. The

general theme in semi-empirical methods is to neglect, or parameterize, the integrals in DFT/HF methods to gain computational speed. In these models, empirical parameters are often added to compensate for the errors due the rather invasive approximations. There are various shades of semi-empirical methods that can be broadly classified as an approximation of either HF based methods or DFT based methods.

The next rung on the multi-scale ladder concerns atoms (cf. Fig. 1.1), and consequently, atomistic models form the next step. At this level, we ignore the electronic degrees of freedom. Energies and forces are evaluated using mathematical expressions that approximate the PES. These mathematical expressions are commonly referred to as force fields (FF). FF simulations are several orders of magnitude faster than QM methods, but are considerably less transferable compared to the electron based models. As a result, different atomic models are developed for various classes of materials. In the following, I will discuss these rungs in more detail.

2.1.1 Electronic structure methods

In the computational materials science community, DFT has emerged as the primary working tool to perform electronic structure calculations. The DFT method greatly simplifies the notion of handling a many-electron system by using its electron density. The Hohenberg-Kohn theorem[16] states that the ground state energy of a system can be exactly determined by the electron density. However, to allow for this, an exact energy functional is required, and such has not yet been discovered. Nevertheless, the available approximations (density functionals) today allow researchers to make accurate predictions of properties and characteristics for a broad class of materials[20].

Despite its tremendous success, standard DFT (local and semi-local functionals) has many limitations, including failure to acccrately describe strongly correlated systems[21,22], inaccurate band gap predictions[23] and high computational cost for modelling systems with many electrons[21,22]. These shortcomings all result in a poor description of properties related to the redox chemistry of metal oxides[24], which is a chemistry of particular interest in this thesis. To overcome some limitations, for example concerning the inaccuracy for correlated systems and electronic band gaps, the DFT+U method (an extension of DFT with a Hubbard U correction), or, a hybrid functional (functionals with a portion of semi-local exchange replaced by non-local Fock exchange) can be used. Such efforts tend to improve the theoretical description of redox systems significantly, albeit at an even higher computational cost. Ideally, an electronic model

with the accuracy of the hybrid DFT, but with a reasonable computational cost is wanted.

In recent years, the self consistent charge density functional tight binding method (SCC-DFTB)[25,26], a semi-empirical approach derived from DFT, has been widely used for electronic structure calculations. The method has been successfully applied to study large biological systems[27], redox chemistry in oxides[28], and electron transport[29] to give some examples. In SCC-DFTB, the Hamiltonian matrix elements are tabulated using a higher level of theory (usually DFT) as a reference, and stored in so-called Slater-Koster (SK) tables. The empirical part commonly referred to as repulsive potential is later added to overcome any shortcomings caused by the parameterization of the Hamiltonian. However, fitting this repulsive potential is often a laborious task, and addressing this problem is one of the primary focus of this thesis.

In this thesis, I have primarily used these two methods for evaluating the electronic structure of materials. In the following, I will go in to more detail concerning the relation (and links) between these two electronic level models.

Density Functional Theory

A rigorous derivation of the DFT method can be found in the following Refs. 30,31. Here, I will go through the basic theory leading to equations that are further expanded on in the SCC-DFTB method. Within DFT, the total energy of a system is a functional of the electron density $n(\boldsymbol{r})$ and can be written as:

$$E[(n(\boldsymbol{r}))] = E^{kin}[n(\boldsymbol{r})] + E^{ext}[n(\boldsymbol{r})] + E^{H}[n(\boldsymbol{r})] + E^{xc}[n(\boldsymbol{r})] + E^{NN}. \tag{2.1}$$

Here, E^{kin} is the kinetic energy of non-intercting electrons, E^{ext} is the energy from the interaction between the nucleus and electrons, E^{H} (the Hartree term) is the energy from the classical electron-electron Coulomb repulsion, E^{xc} is the exchange-correlation energy, as well as corrections to the kinetic energy due to electron-electron interactions, and E^{NN} is the energy from the nucleus-nucleus interaction. In this formulation, all quantities but E^{xc} can be computed readily. As such, the actual functional is defined through the choice if the approximation for E^{xc}. The exact E^{xc} functional is, however, unknown, and there exists a plethora of different approximations for it. Hence, the accuracy of a DFT calculation heavily rely on the choice of E^{xc} functional used. In the literature the different functionals have been classified on the basis of the level of approximations following a Jacob's Ladder towards functional heaven of chemical accuracy[32]. Still, however, the most common density functionals used in the materials science community are the local density approximation (LDA)[17] and various forms of generalized gradient cor-

rections to LDA (so called GGA's)[32] which are found at the base of the ladder.

The insightful idea of Kohn and Sham was to approximate the E^{kin} in Eq. 2.1 using a "single-particle approach" with the help of Kohn-Sham orbitals $\psi_i(\boldsymbol{r})$. The resulting Kohn-Sham equation for a non-interacting system of N electrons is as follows:

$$\begin{aligned} &\left\{ \frac{\nabla^2}{2} + V^{ext} + \int \frac{n(\boldsymbol{r}_2)}{\boldsymbol{r}_{12}} d\boldsymbol{r}_2 + V^{xc}(\boldsymbol{r}) \right\} \Psi_i(\boldsymbol{r}_1) = \epsilon_i \Psi_i(\boldsymbol{r}_1) \\ &\text{and} \quad n(\boldsymbol{r}) = \sum_{i=1}^{N} |\psi_i(\boldsymbol{r})|^2 \end{aligned} \tag{2.2}$$

where ϵ_i are Kohn-Sham orbital energies, V^{ext} is the potential from nuclei, and the exchange-correlation potential is defined as follows:

$$V^{xc}(\boldsymbol{r}) = \frac{\delta E^{xc}[n(\boldsymbol{r})]}{\delta n(\boldsymbol{r})} \tag{2.3}$$

The one-electron Kohn-Sham equations are solved using an iterative method. Initially, a guess density $n(\boldsymbol{r})$ is chosen to compute the orbitals ψ_i using Eq. 2.2. These new orbitals are used to generate the next $n(\boldsymbol{r})$. This procedure is repeated until self-consistency is achieved.

The total energy in DFT in Eq. 2.2 can be written in term of Kohn-Sham orbital energies (ϵ_i) as follows:

$$\begin{aligned} E[(n(\boldsymbol{r}))] = &\sum_{i}^{occ} \epsilon_i - \frac{1}{2} \iint \frac{n(\boldsymbol{r}_1) n(\boldsymbol{r}_2)}{r_{12}} d\boldsymbol{r}_1 d\boldsymbol{r}_2 \\ &- \int V^{xc}[n] n(\boldsymbol{r}) d\boldsymbol{r} + E^{xc}[n] + E^{NN} \end{aligned} \tag{2.4}$$

where i runs over all the occupied orbitals.

The DFT calculations presented in the this thesis primarily utilized semi-local functionals, falling under the class of GGA's discussed above. This type of functional also forms the basis in the SCC-DFTB method described below. All the DFT calculations were performed using the Vienna Ab initio Simulation Package (VASP)[33–36]. A small remark is in place here: the focus of the thesis have been to develop tools to facilitate the coupling and linking in the multi-scale modeling approach, and this tool is agnostic to the method used in the electronic model as well as the software used to solve it.

Self-Consistent Charge Density Functional based Tight Binding

The SCC-DFTB method is a second-order expansion of the KS-DFT energy with respect to the charge density. A detailed derivation of the method can be found in Refs. 26,37.

The ground state density is defined as a perturbation of a reference density $n_0(\boldsymbol{r})$ and using Taylor expansion, the total energy can be written down as follows:

$$E^{SCC-DFTB}[n_0 + \delta n] = E^0[n_0] + E^1[n_0, \delta n] + E^2[n_0, (\delta n)^2] \tag{2.5}$$

with

$$\begin{aligned} E^0[n_0] &= E^{nn} - \frac{1}{2}\iint^{'} \frac{n_0(\boldsymbol{r})n_0(\boldsymbol{r}')}{|\boldsymbol{r}-\boldsymbol{r}'|}d\boldsymbol{r}d\boldsymbol{r}' \\ &\quad - \int V^{xc}[n_0]n_0(\boldsymbol{r})d\boldsymbol{r} + E^{xc}[n_0] \\ E^1[n_0, \delta n] &= \sum_i^{occ} \left\langle \psi_i \middle| \hat{H}[n_0] \middle| \psi_i \right\rangle \\ E^2[n_0, (\delta n)^2] &= \iint^{'} \left(\frac{1}{|\boldsymbol{r}-\boldsymbol{r}'|} + \frac{\delta^2 E^{xc}}{\delta n \delta n'} \right) \delta n(\boldsymbol{r})\delta n(\boldsymbol{r})' d\boldsymbol{r}d\boldsymbol{r}' \end{aligned} \tag{2.6}$$

The first term E^0 is commonly referred to as the repulsive potential energy (E_{rep}). The second term $E^1[n_0, \delta n]$ is the sum of the one-particle energies commonly referred to as the band structure energy (E_{BS}). The third term $E^2[n_0, (\delta n)^2]$ is the second-order correction to the total energy. Using these definitions, the total energy in SCC-DFTB can be written as:

$$E^{total} = E_{BS} + E_{2nd} + E_{rep} \tag{2.7}$$

These energies will be discussed in more detalil in the following.

The band structure energy (E_{BS})
The SCC-DFTB method only explicitly treats the valence electrons, while the core electron interactions are approximated via empirical two-body potentials. The electron orbitals Ψ_i can be expanded in a minimal basis set of valence-only atomic orbitals ϕ_μ within the linear combination of atomic orbitals (LCAO) ansatz as follows:

$$\psi_i = \sum_\mu c_{\mu i}\phi_\mu(\boldsymbol{r}) \tag{2.8}$$

where ϕ_μ is the atomic basis function of orbital μ centered on the atom, and $c_{\mu i}$ are the basis-set coefficients. The atomic orbitals are obtained from a modified Kohn-Sham equation, where an additional confinement

potential (V^{conf}) is added to the Hamiltonian as follows:

$$\left\{\frac{\nabla^2}{2} + V^{\text{atom}}[n(\boldsymbol{r})] + V^{\text{conf}}\right\}\phi_\nu(\boldsymbol{r}) = \epsilon_\nu^{atom}\phi_\nu(\boldsymbol{r})$$

where

$$\begin{aligned} V^{\text{conf}} &= \left(\frac{r}{r_0}\right)^m \\ V^{\text{atom}} &= V^{ext} + V^H + V^{xc}(\boldsymbol{r}) \end{aligned} \tag{2.9}$$

where r_0 is a parameter that needs to be optimised, and usually a quadratic potential ($m = 2$) is used for the confinement. Due to the confinement potential, the resultant atomic orbitals ϕ_ν are compressed, making them more apt to describe chemical bonds in solids and molecules. Additionally, atomic densities are also computed in a similar fashion, but with a different r_0 value.

The following secular equations are obtained to determine the coefficients ($c_{\mu i}$):

$$\sum_\nu c_{\nu i}\left(H^0_{\mu\nu} - \epsilon_i S_{\mu\nu}\right) = 0 \quad \forall\ \mu, i$$

where

$$H^0_{\mu\nu} = \sum_i^{occ}\left\langle \phi_\mu \left| \hat{H}[n_0] \right| \psi_\nu \right\rangle \quad S_{\mu\nu} = \langle \phi_\mu | \psi_\nu \rangle \tag{2.10}$$

where $S_{\mu\nu}$ is the overlap matrix. We can rewrite E_{BS} in Eq. 2.7 in terms of $H^0_{\mu\nu}$ as follows:

$$E_{BS} = \sum_i^{occ}\left\langle \psi_i \left| \hat{H}[n_0] \right| \psi_i \right\rangle = \sum_i^{occ}\sum_{AB}\sum_{\nu\in A}\sum_{\mu\in B} c_{\mu i}c_{\nu i}H^0_{\mu\nu} \tag{2.11}$$

The repulsive energy (E_{rep})

The repulsive energy term in Eq. 2.6 contains to a large extent the core-core repulsive energy, thereby its name. But it also contains exchange-correlation energy, and double counting corrections. It is commonly approximated by an empirical two-body repulsive potential V^{rep} as follows:

$$E^0[n_0] \approx E_{rep} = \frac{1}{2}\sum_{AB} V^{rep}_{AB}(r_{AB}) \tag{2.12}$$

where the indices A and B denote atom indices, r_{AB}=$|\mathbf{R}_A - \mathbf{R}_B|$, and V^{rep} is called the repulsive potential. The V^{rep} is usually short-raged, pairwise additive, and should be defined for all pairs of elements in the system. The parameterization of the repulsive potential is often a laborious and time-consuming task.

The second order energy (E_{2nd})
The fluctuations in charge density is written as a superposition of atomic contributions as:

$$n(\boldsymbol{r}) = \sum_A \delta n_A(\boldsymbol{r}) \tag{2.13}$$

The density fluctuations are approximated by exponentially decaying spherical charge densities with coefficients τ_A

$$\delta n(\boldsymbol{r}) = \sum_A \delta n_A(\boldsymbol{r}) \approx \frac{1}{\sqrt{4\pi}} \sum_A \left(\frac{\tau_A^3}{8\pi} e^{-\tau_A |\boldsymbol{r} - \boldsymbol{R_A}|} \right) \Delta q_A \tag{2.14}$$

The following expression with an analytical function γ is obtained after substituting Eq. 2.14 for E^2 in Eq. 2.6 :

$$E_{2nd} = \frac{1}{2} \sum_{AB} \Delta q_A \Delta q_B \gamma(\tau_A, \tau_B, R_{AB}) \tag{2.15}$$

where Δq is the fluctuation in Mulliken charge on an atom, γ is an analytical function describing charge-charge interaction. At large interatomic distances, the γ function behaves as $\frac{1}{R_{AB}}$, i.e., the E_{2nd} corresponds to the Coulomb energy for the interaction of two point charges Δq_A and Δq_B. When the charges are located on the same atom ($A = B$), γ can be approximated (XC contribution neglected) as the Hubbard parameter U which is twice the chemical hardness of an atom. The Mulliken charges q_A also depends on the ψ_i and should be solved in a self-consistent manner.

All SCC-DFTB calculations performed in this thesis were done with the DFTB+ software[38,39].

2.1.2 Atomistic models

Atomistic models describe the motion of the atoms. The omission of electronic degrees of freedom in atomistic models enable simulations of larger system sizes and time-scales as compared to electronic models. In most atomistic models, motion of the atoms are governed by the laws of Newtonian mechanics, and the forces acting on atoms are obtained using a force field. Force fields are in principle function of the position of all the atomic nuclei present in a system. So, the dimensionality of a force field scales with the system size. However, we can reduce the dimensionality using a many-body expansion as follows:

$$V(r_1, r_2, ...r_n) = \sum_i^N V_{1B}(r_i) + \sum_{i<j}^N V_{2B}(r_{ij}) + \sum_{i<j<k}^N V_{3B}(r_{ij}, r_{jk}, r_{ik}) + \dots \tag{2.16}$$

where V_{1B} is called the one-body interaction, V_{2B} is called the two-body interaction between any pair of atoms, $V_{3B}(r_{ij}, r_{jk}, r_{ik})$ is the interaction between any triplet of atoms. In this thesis, the scope is restricted to two-body force fields. Nevertheless, FFs with varying sophistication have been developed in the literature, some examples are simple two-body potentials for ionic systems, embedded-atom model (EAM)[40] for metals, Tersoff potentials[41] for covalent systems. A major portion of the total energy can be accounted for through two-body interactions. The most popular two-body potentials include the Lennard-Jones potential, Buckingham potential, and Morse potential, to name a few. These potentials have a parametric functional form making them rather inflexible. Therefore, they are often unable to describe interatomic interactions over the whole range of possible atom-atom distances. Additionally, these models are non-linear with respect to the involved parameters, making optimization processes tedious and unnecessarily difficult.

Recent research developments in this area focus on developing non-parametric models[42,43], which in principle are much more flexible compared to the parametric counterparts. However, these non-parametric models lack the in-built physical intuition of the parametric models. Non-parametric models often require large amounts of data to train the potential, and extrapolation to regions outside the training-set can be poor.

2.2 Coupling and linking: electrons-to-atoms

As discussed in the introducion, challenges in materials chemistry are truly multi-scale in nature, i.e., an array of simulations using different entities is often required. In particular, the electronic-to-atomistic linking by force fields is of major interest for this thesis.

A major challenge in linking is the transfer of information from one model to the other. The steps involved in linking, in particular, for force fields are described below:

1. Collection of reference data, either from experiments or from QM models
2. Specify choice of representation: two-body, three-body, etc.
3. Specify functional form: parametric (Buckingham, Morse) or non-parametric (splines, polynomials, etc.)
4. Define the objective function and specify methods for optimisation.

Typically, the reference data in step (i) includes: energies, forces, structural parameters, charges, etc., which in the multi-scale approach are derived from QM calculations. The choice of representation in step (ii), depends on the system under investigation. For example, two-body potentials are known to well describe ionic systems, but fails for met-

als and covalent systems were a higher order representation is required (cf. Eq. 2.16). The choice of functional form in step(iii), significantly influences the accuracy and transferability of the generated FF model.

Over the years, parametric FFs have become very complex with often non-intuitive, correlated, and non-linear parameters introduced to tackle problems in transferability and accuracy, and thereby making the models usable for a wider range of materials. However, an increased complexity of the FF model neither guarantees an increased transferability nor increased accuracy. Additionally, non-linear optimisation techniques needed to determine the parameters (step (iv)) does not guarantee a globally optimal solution, and often one resorts to manual tweaking of the parameters based on prior knowledge. The aforementioned problems are clear bottlenecks in efforts aiming at linking electronic and atomistic models, and effectively prevents an efficient implementation of multiscale workflows. Some strategies and directions on how to improve this will be given in the following section.

2.3 Mathematical methods

Mathematical optimisation, or mathematical programming problems, are ubiquitous in all the disciplines of science. Optimisation problems generally consist of unknown variables (decision variables), an objective function, and possibly, constraints. Optimisation problems can be broadly divided into two classes, namely, unconstrained and constrained optimisation. As the names suggest, there are no constraints on the unknown variables in unconstrained optimization, while if constraints are present, it is called constrained optimisation. There are various classes of constrained optimisation problems, which include convex programming problems, QP problems, non-linear programming problems, to name but a few.

In connection to electronic-to-atomic linking, FF parameters are obtained through optimisation towards certain reference values (see step (i) in the previous section). The quality of a FF naturally depend on the choice of mathematical expressions used to describe interactions but also strongly depend on how well the parameters in these expressions have been optimized (steps (iii) and (iv) in the previous section). So, it is of utmost importance to obtain the optimal parameters. In general, most of the FF optimisation problems fall under the class of non-linear least squares problems, a special case of unconstrained optimisation problems. The solutions to non-linear problems cannot be expressed in a closed form format and numerical optimisation procedures are required. Even though there are numerous efficient algorithms to carry out such

optimizations, the global minimum is hard to find due to the existence of multiple local (false) minima.

In contrast, if the FF parameters depended linearly on the FF functional form, the optimal solution could be written down in a closed form expression. This is the case for the FF formulation developed and used in this thesis where the FF optimisation problem fall under the class of convex QP problems, for which a global minimum can be found with certainty. The definitions and advantages are described in the subsequent sections.

2.3.1 Convex optimisation

The standard form for a convex optimisation problem can be written as[44]:

$$\begin{aligned} \min \ & f(x) \\ \text{subject to } & g_i(x) \leq 0 \\ & h_j(x) = 0 \end{aligned} \tag{2.17}$$

The above optimisation problem is convex if the objective f is convex, the inequality constraints g_i are all convex functions, and the equality constraints h_j are all affine funtions. Note that the above definition is an explicit formulation. In a sense, a more implicit definition is that the objective function is minimised over a convex set. Convex optimisation has some useful properties:

- local minimisation is equivalent to global minimisation
- For a strictly convex objective function (f), there is at most one optimal point.

2.3.2 Quadratic programming

In a QP problem, the objective function is quadratic in the decision variables, with linear equality and inequality constraints. This class of numerical optimisation problems are common in curve fitting. The standard form can be written as:

$$\begin{aligned} \min_{\boldsymbol{x}} \ & \frac{1}{2}\boldsymbol{x}^T\boldsymbol{P}\boldsymbol{x} + \boldsymbol{q}^T\boldsymbol{x} \\ \text{subject to } & \boldsymbol{G}\boldsymbol{x} \leq \boldsymbol{h} \\ & \boldsymbol{A}\boldsymbol{x} = \boldsymbol{b} \end{aligned} \tag{2.18}$$

where matrix $\boldsymbol{P}$ and $\boldsymbol{q}$ denotes the quadratic function to minimze, matrix-vector tuple ($\boldsymbol{G}$,$\boldsymbol{h}$) and ($\boldsymbol{A}$,$\boldsymbol{b}$) correspond to inequality and equality constraints and $\boldsymbol{x}$ is the decision variables. A problem is convex when the matrix $\boldsymbol{P}$ (Hessian) is at least positive semi-definite.

2.3.3 Linear least squares

A linear least squares problem is the same as a convex QP problem. A standard linear least-square can be written down as follows:

$$\begin{aligned} J(\boldsymbol{x}) &= \frac{1}{2} \left\| \boldsymbol{R}\boldsymbol{x} - \boldsymbol{s} \right\|^2 \\ &= \frac{1}{2}\boldsymbol{x}^\top \boldsymbol{R}^\top \boldsymbol{R}\boldsymbol{x} - \boldsymbol{s}^\top \boldsymbol{R}\boldsymbol{x} + \frac{1}{2}\boldsymbol{s}^\top \boldsymbol{s} \end{aligned} \tag{2.19}$$

The last term in Eq. 2.19 is a constant, so minimisation of $J(\boldsymbol{x})$ is the same as:

$$J(\tilde{\boldsymbol{x}}) = \frac{1}{2}\boldsymbol{x}^\top \boldsymbol{R}^\top \boldsymbol{R}\boldsymbol{x} - \boldsymbol{s}^\top \boldsymbol{R}\boldsymbol{x} \tag{2.20}$$

This is now a standard QP problem with $\boldsymbol{P} = \boldsymbol{R}^\top \boldsymbol{R}$ and $\boldsymbol{q} = -\boldsymbol{R}^\top \boldsymbol{s}$. A simple inspection reveals that the matrix $\boldsymbol{P}$ is positive semi-definite. Hence, linear least squares problem are convex QP problem.

3. Paper I: Development of the CCS method

Purposes:
- To develop a flexible, non-parametric, and parameterization friendly two-body force field.
- To package the method into user-friendly software.

Methods: DFT, QP

Take-home message: An efficient method called Curvature Constrained Splines (CCS) was developed to construct two-body potentials. The two-body potentials are constructed using cubic splines subjected to constraints on the curvature. The objective function is convex, and the spline coefficients can be obtained using a QP approach.

3.1 Motivation

A major challenge in multiscale modelling of materials is the transfer of information between scales, i.e., linking various levels of theory [14]. In this chapter, the focus is on electronic-to-atomistic linking through the use of force field models, in which electronic degrees of freedom are omitted to gain computational speed. The following question is addressed — Is it possible to construct non-parametric two-body potentials with a built-in chemical intuition, and at the same time, are easy to parameterize?

In **Paper I**, a methodology based on the use of curvature constrained splines (CCS) was developed to facilitate the generation of flexible, accurate, and parameterization friendly two-body potentials. The central tenet of the CCS method is to stipulate the cubic splines as a function of curvature (second derivative) and impose constraints to mimic key features of the parametric two-body potentials. The constraints, in a manner, impart the "chemistry" into the CCS model. The methodology was implemented as a python package, freely available at `https://github.com/aksam432/CCS`

3.2 CCS in a nutshell

Consider a pair of interacting atoms, with interatomic distances varying over a range $[r_{\min}, r_{\text{cut}}]$. The interval is subdivided into N equal sub-

intervals with $I_n = [x_{n-1}, x_n]$, for $n = 1, \ldots N$. Cubic spline functions are defined on each sub-interval as follows:

$$f_n(x) = a_n + b_n(x - x_n) + \frac{c_n}{2}(x - x_n)^2 + \frac{d_n}{6}(x - x_n)^3. \tag{3.1}$$

The x_n are called knots and there are N+1 knots in total with $x_n = r_{\min} + n\Delta x$, where $n = 0, \ldots N$, and $\Delta x = (r_{\text{cut}} - r_{\min})/N$. In a standard cubic spline approach interpolation conditions are imposed on the the spline function and continuity conditions on the first and second derivative functions. Here, interpolation conditions are imposed on the second derivative functions to get the following $2N$ conditions:

$$\begin{aligned} f_n''(x_{n-1}) &= c_{n-1}, \quad \text{for } n = 1, \ldots, N, \\ f_n''(x_n) &= c_n, \qquad \text{for } n = 1, \ldots, N. \end{aligned} \tag{3.2}$$

The curvature values (c) are later optimised to get the best potential. However, before doing following $2N-2$ continuity conditions are imposed as shown below:

$$\begin{aligned} f_n(x_n) &= f_{n+1}(x_n), \quad \text{for } n = 1, \ldots, N-1, \\ f_n'(x_n) &= f_{n+1}'(x_n), \quad \text{for } n = 1, \ldots, N-1, \end{aligned} \tag{3.3}$$

There are $4N$ unknowns but only $4N - 2$ conditions. To uniquely determine f, the following 2 boundary conditions as imposed:

$$f_N(x_N) = f_N'(x_N) = 0. \tag{3.4}$$

Using the above relations, we can show that coefficients $\boldsymbol{a} = [a_1, a_2, \ldots, a_N]^T$ $\boldsymbol{b} = [b_1, b_2, \ldots, b_N]^T$ and $\boldsymbol{d} = [d_1, d_2, \ldots, d_N]^T$ are linearly dependent on the curvatures $\boldsymbol{c}$.

3.2.1 Optimization problem

The energy of a system can be written down as follows:

$$E^{CCS} = \boldsymbol{v}^\top \boldsymbol{c} + \boldsymbol{w}^\top \boldsymbol{\epsilon}, \tag{3.5}$$

where $\boldsymbol{v}$ is a feature vector containing structural information (pairwise distances), $\boldsymbol{c}$ is a vector with curvature value at the endpoint of each subinterval, $\boldsymbol{w}$ is the number of atoms of each chemical species in the system, and $\boldsymbol{\epsilon}$ is a vector containing the one-body energy of each chemical species.

Consider K number of chemical configurations. Then, the objective function is optimized over a diverse set of such configurations k=1...K,

a so-called training-set, in a least-square sense and can be written as follows:

$$\begin{aligned} J &= \frac{1}{2}\sum_{k=1}^{K}\left(E_k^{\mathrm{CCS}} - E_k^0\right)^2, \\ &= \frac{1}{2}\sum_{k=1}^{K}\left(\boldsymbol{v}_k^\top \boldsymbol{c} + \boldsymbol{w}_k^\top \boldsymbol{\epsilon} - E_k^0\right)^2 = \frac{1}{2}\|\boldsymbol{V}\boldsymbol{c} + \boldsymbol{W}\boldsymbol{\epsilon} - \boldsymbol{e}^0\|_2^2. \end{aligned} \tag{3.6}$$

where $\boldsymbol{V} \in \mathbb{R}^{K\times N+1}$ has rows $\boldsymbol{v}_k$, the K-vectors of energies $\boldsymbol{e}^0$, and $\boldsymbol{W}$ contains rows $\boldsymbol{w}_k$. As shown in section 2.3.3, least-square problems can be cast into a standard QP problem. The python package CVXOPT[45], was used to solve the QP problem.

3.2.2 Constraints

The CCS method can be used to tune the shape of the fitted potential using constraints on the curvature value at the endpoint of each subinterval. The user can construct a set of constraints required for a particular system based on prior knowledge. Some important examples of the so far implemented constraints are illustrated in Fig. 3.1, and are discussed in some detail in the list below.

Repulsive constraint

This set of constraints ensure that the fitted spline potential is completely repulsive, cf. Fig. 3.1(a). This is ensured by having positive values for all $\boldsymbol{c}$ coefficients, and the corresponding constraint matrix is shown in Eq. 3.7. In **Paper III** these constraints were used to fit the repulsive potentials in the SCC-DFTB method. The interaction between two atoms is purely repulsive when they are close to each other (Pauli repulsion). Therefore, the repulsive constraint can also be used to model short-ranged interactions.

$$\boldsymbol{G}^{\mathrm{repulsive}} = -\boldsymbol{I}_{N+1} \quad \text{and} \quad \boldsymbol{h} = \boldsymbol{0}_{(N+1)\times 1}. \tag{3.7}$$

Monotonous constraint

The repulsive constraint only ensures that the $\boldsymbol{c}$ coefficients are positive. However, the $\boldsymbol{c}$ coefficients can vary too rapidly between knots, leading to poor frequencies and forces. The noise in $\boldsymbol{c}$ coefficients for spline potentials was also reported by Gaus *et al.*[46]. The monotonous constraint curbs such effects by having a tighter constraint on $\boldsymbol{c}$ coefficients

as shown in Eq. 3.8 and illustrated in cf. Fig. 3.1(b).

$$\boldsymbol{G}^{\text{monotonous}} = \begin{bmatrix} -1 & 1 & 0 & \dots & 0 \\ 0 & -1 & 1 & \dots & 0 \\ \vdots & & \ddots & & \vdots \\ 0 & 0 & 0 & -1 & 1 \end{bmatrix} \quad \text{and} \quad \boldsymbol{h} = \mathbf{0}_{N\times 1}. \tag{3.8}$$

Switch constraint
In general, most parametric two-body potentials has two regions: a convex region from (r_{min} to r_{switch}) and a concave region from (r_{switch} to r_{cut}). To capture this functional form, the following constraints are employed:

$$\begin{aligned} c_i &\geq 0 \text{ for } i < N_{\text{switch}}, \\ c_i &\leq 0 \text{ for } i \geq N_{\text{switch}}. \end{aligned} \tag{3.9}$$

This constraint was used in **Paper I** to generate a two-body potential for neon and is schematically illustrated in Fig. 3.1(c).

$$\boldsymbol{G} = \begin{bmatrix} -\boldsymbol{I}_{N_1} & \mathbf{0}_{N_1\times N_2} \\ \mathbf{0}_{N_2\times N_1} & \boldsymbol{I}_{N_2} \end{bmatrix} \quad \text{and} \quad \boldsymbol{h} = \mathbf{0}_{(N+2)\times 1}, \tag{3.10}$$

Sparse constraint
The spline grid is assumed to be equally spaced over an interval in the CCS method. However, when a fine grid is used, there might be regions in the interval that lacks data. The curvature values at such grid points are ambiguous. There are several methods to remove this ambiguity. One approach is to remove the redundant knots with sub-interval merging, as illustrated in Fig. 3.1(d), to minimize the curve (arc) length for curvatures over the ambiguous sub-interval domain.

Mixed constraint
It is often useful to combine the aforementioned constraints to get a reliable potential. For example, in **Paper III** the repulsive and monotonous constraints were combined to curb the oscillations in curvature values. Similarly, the switch and monotonous constraints were combined in **Paper II**. Essentially, the user has full freedom to design custom constraints and combine them with the CCS machinery.

3.3 Validation on neon ab initio data

As an initial test, to validate the CCS method, two-body interatomic potentials were developed for bulk solid neon. A data set that included both isotropic bulk scans and scrambled bulk neon structures was created. The training-set comprised of 90 % of the data, and the rest were

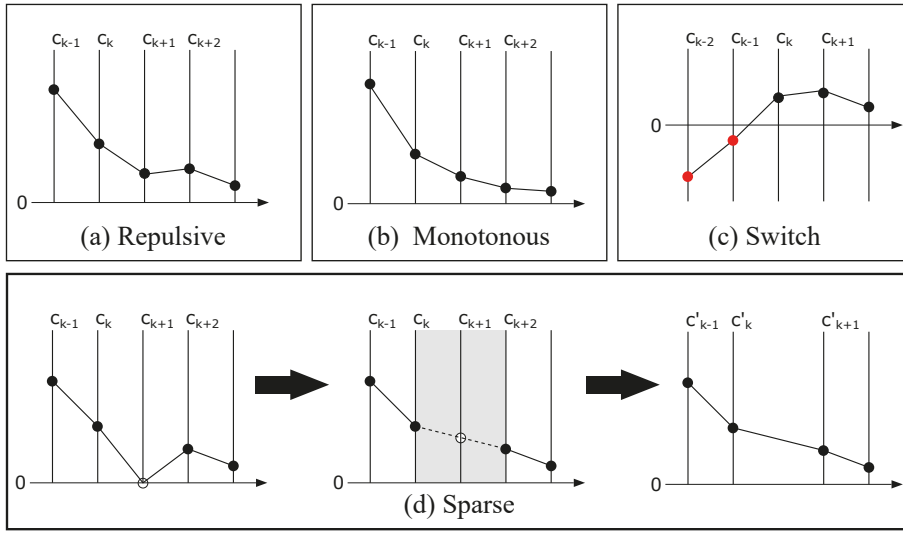

Figure 3.1. An illustration of the various constraints used in the CCS method. The black dots and red dots indicate positive and negative curvature values, respectively.

used in the test-set to validate the quality of the potential. The extent of over-fitting in a model can be qualitatively understood by comparing the error in the fitting and validation data. The unconstrained cubic splines and CCS were used to fit the data, and the results are shown in Fig. 3.2. The unconstrained cubic splines show clear signs of overfitting, i.e., the training-set error decreases while the test-set error increases with an increase in the number of knots (parameters), as seen in Fig. 3.2. On the contrary, no sign of overfitting is seen for CCS, where the test-set error and training-set error converge as we increase the number of knots. The constraints in the CCS method ensures that noise in the training-set is not captured by the model. Fig. 3.3 shows the comparison between two-body potentials for both the methods using 10 knots. Small oscillations in the unconstrained cubic spline potential are seen even at 10 knots.

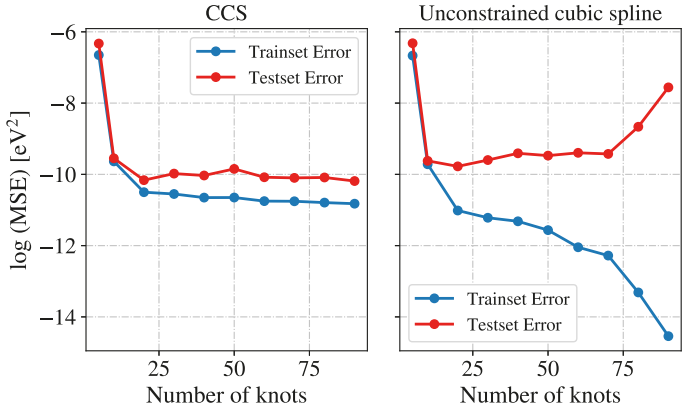

Figure 3.2. The error in the training-set (blue) and the test-set (red) data are shown for both the CCS and unconstrained cubic spline. The x-axis shows the number of knots in the spline interval. The y-axis shows the logarithm of mean squared error (MSE).

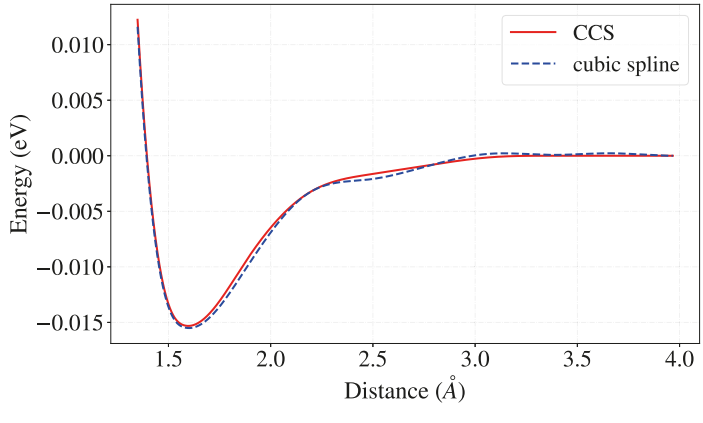

Figure 3.3. A comparison between two-body potentials generated using the CCS method and unconstrained cubic splines using 10 knots.

4. Paper II: CCS+Q method for ionic materials

Purposes:
- To extend the CCS method for multicomponent fitting and ionic systems with the inclusion of long-range Coulomb interactions.
- Analyse performance of the extended method for bulk ZnO and CeO_2 nanoparticles.

Methods: DFT, Buckingham and CCS+Q
Calculated properties: energy-volume curves, lattice parameters, bulk modulus, charges, and nanoparticle formation energies.
Take-home message: We showed that the CCS+Q model, an extension of CCS, is a better alternative than commonly used Buckingham/Born Mayer models for ionic systems. The CCS+Q method is superior in terms of flexibility, accuracy, and ease of optimisation. We demonstrated that all the parameters, including charges, could be solved using a standard QP approach. The transferability of the CCS+Q model is well illustrated with the accurate prediction of change in morphology in CeO_2 nanoparticles.

4.1 Why extend the CCS method?

In **Paper I**, the theory and software package for the CCS method was developed, and the key features of the method were demonstrated. It is, however, recognised that two limiting assumptions were used while deriving the formalism for the CCS method that hinders effective use of the method: *i)* it was made for single-component systems, and *ii)* long-ranged electrostatic interactions are neglected. In the following work, both these issues are dealt with.

Chemical systems are often complex, with two or more atomic species, and usually involve charge transfer between the different chemical species. In such systems, electrostatic interactions play a crucial role, which cannot be captured by the CCS method. Moreover, a system with N different atomic species has $\binom{N}{2}$ pairs and hence require us to determine equally many two-body potentials. Consequently, the optimisation process becomes tedious, even for simple non-linear Lennard-Jones or Buckingham

models, and at times require computationally heavy and resource-hungry evolutionary algorithms.[47,48]

In **Paper II**, the CCS+Q method was introduced as an extension of the CCS methodology, with scaled charges (Q) to include electrostatic interactions and the possibility to handle multi-component systems. The multi-component problem retained both the linearity of the model and the convexity of the objective function, similar to the single component case.

4.2 How to optimise the charges?

We chose metal oxides (ZnO and CeO_2) as candidate systems to validate the CCS+Q method. In metal oxides, the interatomic interactions are dominated by electrostatic interactions between the anions and cations. The inclusion of a simple point charge model has been shown to provide a qualitative understanding of the underlying chemistry of such systems[49–51]. However, a question still pertains—How to determine the value of the point charges?

The electron density in solids can be measured from diffraction experiments or be computed theoretically from QM calculations. Since charge, unlike electron density, is not an observable, there is no unambiguous way to assign the charge, and the value depends on the model we choose to derive it. There are broadly two ways to determine charges for metal oxides: *i)* from experimental data[52,53] *ii)* from QM data[54–58]. There are several QM based methods, which include: Mulliken, and Löwdin population analyses[54,55], Hirshfeld decomposition[56], density derived electrostatic and chemical (DDEC) charges[59], the electrostatic potential (ESP) derived charges[57,58], to name a few. However, there is little clarity when picking a model to derive charges for a force field. Nevertheless, we used the DDEC approach in **Paper II**.

We proposed two ways to fit the charges under the CCS+Q scheme: *i)* CCS with DDEC charges (denoted as CCS+DDEC), and *ii)* CCS with scaled charges (denoted as CCS+SQ). In the latter approach, charges are considered as parameters and are optimised to get the correct DFT energies. Initially, formal charges are assigned to the ions and are scaled using an optimal scaling factor ($\alpha = \sqrt{\gamma}$). The scaling factor is optimised with other spline coefficients in a linear fashion. The expression for the objective function is as follows:

$$J = \frac{1}{2} \| \underbrace{\boldsymbol{M}\boldsymbol{c} + \boldsymbol{W}\boldsymbol{\epsilon}}_{CCS} + \boldsymbol{Q}_f \gamma - \boldsymbol{e}^{\mathrm{ref}} \|_2^2 \tag{4.1}$$

where $\boldsymbol{M}$ is the feature matrix containing structural information, $\boldsymbol{W}$ is the stoichiometry matrix, $\boldsymbol{Q_f}$ contains electrostatic energy using formal

charges, and $\boldsymbol{e}^{\text{ref}}$ is the reference energy values. The spline coefficients $\boldsymbol{c}$, one-body energy $\boldsymbol{\epsilon}$, and γ are the unknowns in Eq. 4.1. A detailed derivation and the constraints used can be found in **Paper II**. The optimised charges are then used to evaluate electrostatic energy contribution via Ewald summation.[60]

4.3 Multicomponent fitting using CCS+Q

4.3.1 ZnO

The initial step to parameterize a force field is the construction of a training-set. In this work, we have chosen to include Energy-Volume (E-V) scans for the following 4-coordinated polymorphs of ZnO — wurtzite (WZ), zincblende(ZB), cubane, and body-centered tetragonal (BCT). We evaluated the performance of the CCS+DDEC and Buckingham models combined with charges derived from QM-calculations using the DDEC method, as well as the CCS+SQ model with optimized charges, for the structures included in the training-set. The DDEC charges were derived from the GGA optimised wurtzite structure, being $\pm 1.31e$. The optimised charges in the CCS+SQ model were optimized for the whole training set to $\pm 1.14e$. The resulting Zn-O, Zn-Zn, and O-O potentials are shown in Fig. 4.1. The corresponding E-V curves for the structures in the training-set using all three models are shown in Fig. 4.2. Despite the dissimilar short-range potential forms, the E-V curves are well captured by all three models when compared to the reference DFT data, which is consistent with the fact that the Coulomb interaction is the primary contributor to the total energy (about an order of magnitude at a distance of 4Å). However, as the devil is often in the details, the data could also suggest that there is overlap in the short-ranged interaction description, i.e., repulsion in the Zn-O bond can be compensated by spurious attraction in the O-O and Zn-Zn, and constitutes a problem with multi-component fitting procedures. However, within linear models such as CCS+Q, such overlaps can be quantified and avoided by using a clever training-set design or by the use of smart constraints. In fact, a closer inspection of the boxplots presented in Fig. 4.3a reveal that the average training-set error is in the following order: $E_{CCS+SQ} < E_{CCS+DDEC} < E_{Buckingham}$. This illustrates the benefit of the increased flexibility of the CCS+Q functional form over one of the more rigid Buckingham model.

To test the transferability of the generated models, we additionally considered two extra polymorphs, namely the Rock-Salt (RS) and CsCl structural forms of ZnO. These structures are denser compared to the structures included in the training set, and consequently, the Zn ion coordination is increased (6 and 8 for RS and CsCl, respectively).

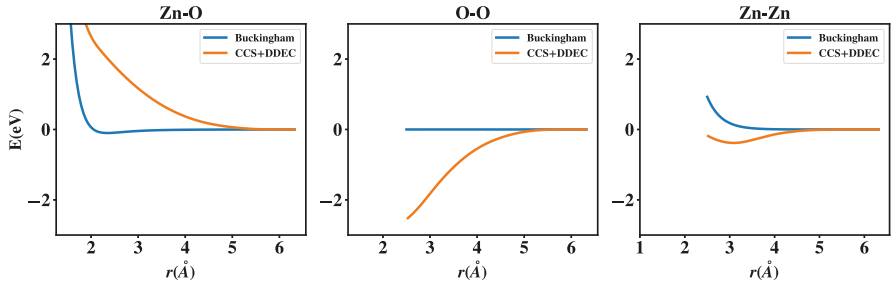

Figure 4.1. The interatomic potentials (excluding the 1-body and Coulomb contributions) for ZnO using both CCS+Q (orange) and Buckingham (blue) are shown above. The left panel shows Zn-O potential, the middle panel shows O-O potential, and the right panel shows Zn-Zn potential.

The table 4.1 contains the calculated lattice parameters, total energy, and bulk moduli for all considered ZnO polymorphs. The lattice parameters and bulk moduli of polymorphs in the training-set were well reproduced by both the CCS+Q and Buckingham models. However, we found the accuracy of CCS+DDEC better for structural properties than CCS+SQ (see Fig. 4.3b). For the test-set structures, all three models gave poor quantitative predictions for energy and structural properties. However, in terms of the relative stability trend for the various polymorphs, the CCS+Q models reproduced the correct order $E_{WZ} < E_{ZB} < E_{BCT} < E_{RS} < E_{CsCl}$ when compared to the reference DFT data. Here, the Buckingham potential, trained on the same structures gave the following order: $E_{WZ} \sim E_{RS} < E_{ZB} \sim E_{BCT} < E_{CsCl}$. The origin of the discrepancies found here (both quantitative and qualitative) lies in that the structures in the test-set are, as mentioned above, quite different from the structures in the training-set. Consequently,

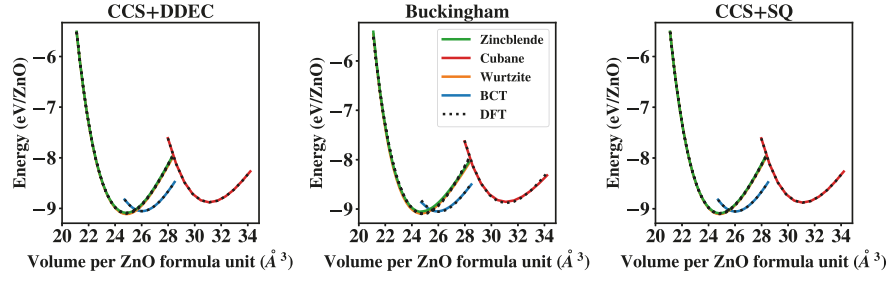

Figure 4.2. A comparison of E-V curves between CCS+Q (left) and Buckingham model (right) are shown for Zincblende (green), Cubane (red), Wurtzite (orange), and BCT (blue). The corresponding DFT values are shown in black.

extrapolation to regions that are neither explored by CCS+Q nor the Buckingham potential. These results highlight the need to emphasize on the importance of diversity among the training-set structures, not only its size, i.e., number of structures. Currently, the construction of a reliable training-set is more of an art than science. However, properties of linear models, like the ones presented herein, could be utilized in the future to make the process more robust.

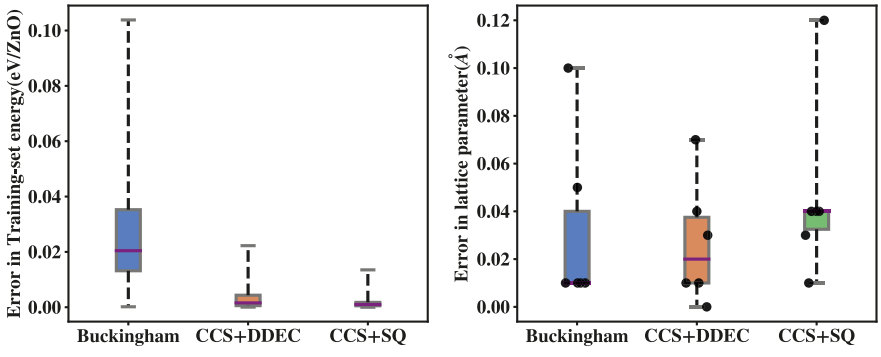

Figure 4.3. Comparison of the quality of the fit for the three ZnO models. The boxplot to the left shows the error in energies per formula unit for the structures in the training-set for both Buckingham (blue), CCS+DDEC (orange) and CCS+SQ (green) potential. The boxplot to the right compares the error in lattice parameters in the training-set (black dots). The whiskers of the boxplot indicate the minimum and maximum error, and the median is shown in purple.

4.3.2 CeO_2

We further tested the CCS+Q methodology on CeO_2 nanoparticles. Ceria nanoparticles are known to have different morphologies based on their size. In particular, small ceria nanoparticles (Ce_nO_{2n}) < 2 nm prefer a tetrahedral shape compared to larger nanoparticles, which are octahedral[61]. A schematic illustration of the CeO_2 nanoparticles is shown in Fig.4.4.

In general, nanoparticles are more challenging to model using force fields than bulk structures due to the variations in coordination number of atoms (bulk vs. surface vs nanospecific motifs). Consequently, a more structurally diversified training-set than the one used for the ZnO parameterization presented above is needed. The training-set used here includes scrambled bulk fluorite CeO_2 structures (111 in total), isotropic scans of thin [111] surface slabs (11 in total), and 2 small nanoparticles of different shapes.

Table 4.1. *The total energies, lattice parameters, and bulk modulii for studied ZnO polymorphs computed using the reference method DFT-PBE and the CCS+DDEC, CCS+SQ and Buckhingam potentials.*

	PBE	CCS+DDEC	CCS+SQ	Buckingham
Wurtzite				
a[Å]	3.29	3.32	3.33	3.30
c[Å]	5.30	5.23	5.18	5.20
E[eV]	-9.10	-9.12	-9.12	-9.09
B[GPa]	129	136	146	123
Zincblende				
a[Å]	4.63	4.64	4.64	4.62
E[eV]	-9.09	-9.09	-9.09	-9.06
B[GPa]	129	131	134	124
BCT				
a[Å]	5.63	5.62	5.59	5.58
c[Å]	3.29	3.32	3.33	3.30
E[eV]	-9.05	-9.06	-9.06	-9.06
B[GPa]	105	112	116	111
Cubane				
a[Å]	6.29	6.33	6.32	6.28
E[eV]	-8.88	-8.93	-8.91	-8.89
B[GPa]	97	89	86	91
RS				
a[Å]	4.34	4.40	4.53	4.28
E[eV]	-8.81	-8.43	-8.22	-9.09
B[GPa]	166	41	53	163
CsCl				
a[Å]	2.69	2.69	2.77	2.68
E[eV]	-7.68	-6.95	-6.48	-7.78
B[GPa]	160	102	48	140

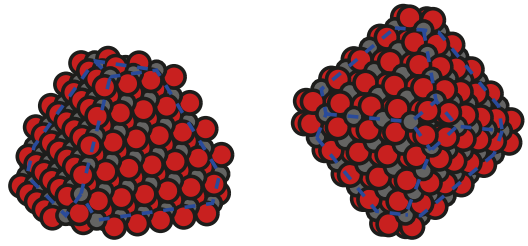

a) $Ce_{113}O_{226}$ tetrahedra b) $Ce_{140}O_{280}$ octahedra

Figure 4.4. (a) Tetrahedral and (b) octahedral CeO_2 nanoparticles. Cerium and oxygen atoms are depicted in gray and red colors, respectively.

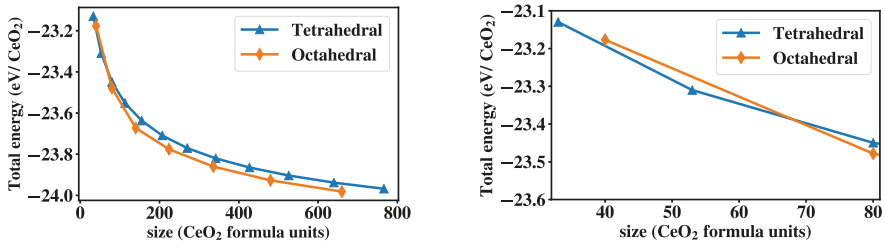

(a) *(b)*

Figure 4.5. Comparison of total energies per formula unit for nanoparticles of tetrahedral and octahedral shape using CCS+Q. (a) Plot covering the whole range of nanoparticles considered in the current work. (b) Plot showing the region where the crossing from tetrahedral to octahedral stability takes place.

After the fitting of CCS+Q Ce-O, Ce-Ce, and O-O potentials, we used the model to compute the geometry and total energy for a series of tedrahedrally and octahedrally shaped ceria nanoparticles. Fig. 4.5a compares the total energy per formula unit as a function of its size. To validate the model, we compare it with the tetrahedral-to-octahedral transition, which in the literature has been reported to occur for sizes of ∼70-80 formula units[61]. The result of the CCS+Q method is in very good agreement with this prediction, cf. Fig. 4.5b. This example demonstrates that the CCS+Q model indeed is flexible enough to capture the diversity that is expected to be encountered when studying complex chemical problems. Adding the relatively simple parameterization process to this, we anticipate that the CCS+Q model can become an increasingly useful tool in many aspects of multiscale materials modeling.

5. Paper III: CCS as repulsive potential in the SCC-DFTB method

Purposes:
- To use the CCS methodology to fit repulsive potentials in the SCC-DFTB method.
- Highlight the transferability issues due to a two-body repulsive potential in the SCC-DFTB method.
- Present neural networks as a possible solution for a transferable repulsive potential.

Methods: DFT, DFTB, CCS, BPNN

Take-home message: The CCS methodology was used to fit two-body repulsive potentials in the SCC-DFTB method. However, due to the approximations in the SCC-DFTB method, the transferability of the two-body repulsive potentials is limited. In regard to transferability, the repulsive potentials should include many-body effects, possibly in the form of local coordination numbers of the atoms. In this context, the Behler-Parinello Neural Networks (BPNN) could be a possible solution in the future.

5.1 Motivation

Though atomistic models (force field methods) like CCS+Q are quite useful, a large part of the chemistry, for example, in describing reducible oxides, requires knowledge about the electronic structure, which is only implicitly treated in atomistic models. In the multiscale modelling approach, there is indeed a need also for an intermediate level of theory that is computationally cheaper than DFT but still capable of providing accurate electronic structures. The SCC-DFTB method is one such tool, which strikes the right balance between computational speed and accuracy when compared to DFT and FF approaches. However, the parameterization, i.e., the generation of Slater-Koster tables with corresponding accurate two-body repulsive potentials, can be very time-consuming.

The repulsive potentials used in the SCC-DFTB method are generally short-range two-body potentials that approximate core-core interaction. However, all the complicated physics and approximation errors that are

explicitly treated in the reference method (usually semi-local DFT) are hidden in the repulsive potentials. As such, it resembles the exchange-correlation term in DFT (see section 2.1.1), but at another scale. Consequently, the repulsive potential does not have a physically motivated shape, making it hard to parameterize. The transferability and reliability of the SCC-DFTB method are heavily dependent on the quality of the underlying two-body repulsive potentials.

Several semi-automated methods have been developed in the literature for fitting repulsive potentials,[37,46,62–68] but each has its own drawbacks or require some form of manual intervention. The currently used methods can be classified into two types: *i)* functions with a rigid functional form (e.g., Buckingham, exponential functions, etc.) *ii)* functions without functional form (e.g., using splines[46,62]). The former methods are not flexible enough, and the latter methods are too flexible and can result in overfitting. Therefore, in **Paper III** the extended CCS methodology introduced in **Paper II** was used, but without the long-ranged electrostatics, for repulsive potentials in the SCC-DFTB method.

5.2 A repulsive fitting for Si using CCS

To demonstrate how the CCS methodology can be used in conjunction with the SCC-DFTB formalism, repulsive potentials were fitted for the following polymorphs of Si: Graphene (3 coordinated), Diamond (4 coordinated), simple cubic (SC, 6 coordinated), and Body-Centered Cubic (BCC, 8 coordinated). The training-set consisted of Energy-Volume (E-V) scans of all polymorphs, with nearest-neighbor Si distances varying between 2.1 to 3.3 Å (see Fig. 5.1). The electronic part of the SCC-DFTB energy for Si was obtained using the *siband* Slater-Koster tables[69,70]. The repulsive potential in SCC-DFTB is usually assumed to be short-ranged (including the first nearest neighbor); however, the use of long-ranged potentials have been reported in the literature[71]. The CCS methodology can be used to actually determine the optimal cut-off required for the repulsive potential given a particular training set. The results from such an optimization is shown in Fig. 5.1. The results indicate that the optimal cut-off indeed is short-ranged for the used training-set. A cut-off value of 3.4 Å—including all the first nearest-neighbors — was sufficient for the repulsive potential (see Fig. 5.1).

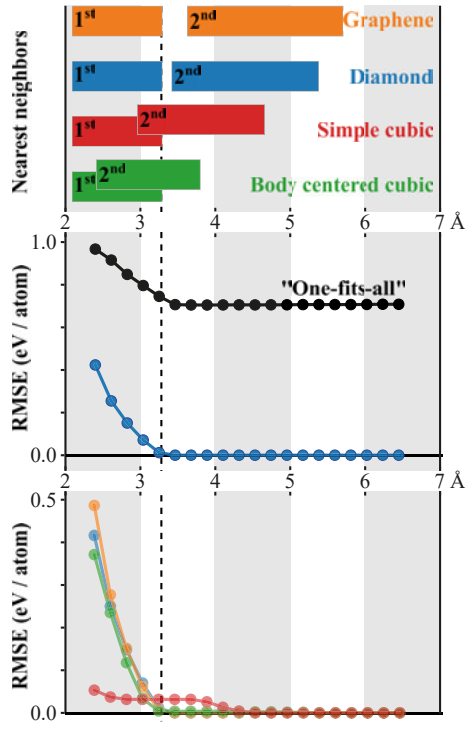

Figure 5.1. The range of first and second nearest-neighbour distances for the Si polymorphs, namely, graphene (orange), diamond (blue), SC (red), and BCC (green) are shown in the top panel. The middle panel depicts the root-mean-squared-error (RMSE) as a function of cut-off radius for diamond (blue) and all polymorphs (black). The bottom panel shows the same for individual polymorphs. The vertical line (dashed) at 3.3 Å indicates the largest nearest-neighbour distance in the training-set.

Unlike what the name suggests, the repulsive potential in SCC-DFTB need not always be a purely repulsive function. The potential can have attractive regions as well[46,71]. Therefore, we used both repulsive and switch constraints in the CCS method to fit the repulsive potentials (see Fig. 5.2). We observed that the shape of the ideal repulsive potential varies for each polymorph. The high-coordinated structures (BCC and SC) require an attractive function in the repulsive potential, whereas purely repulsive functions were obtained for the diamond and graphene polymorphs. We could not obtain a one-fits-all repulsive potential that gave a universal agreement of DFT and SCC-DFTB across all polymorphs. This further highlights the known transferability problems in SCC-DFTB[65].

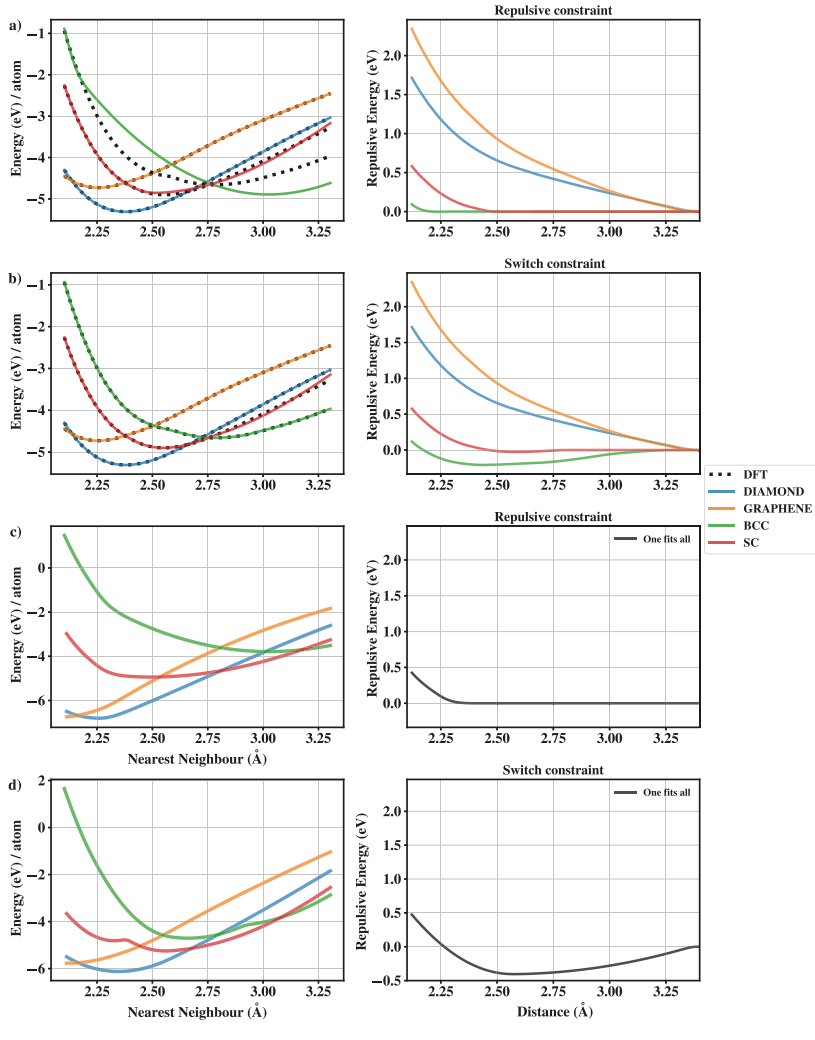

Figure 5.2. The left panel in a) compares DFT energies (black dotted lines) with SCC-DFTB energies using repulsive constraints for all structures in the training-set. The right panel in a) shows the corresponding repulsive potentials. Panel b) shows a similar comparison to that of panel a) for the switch constraint. Panels c) and d) show the repulsive potential obtained using repulsive and switch constraint, respectively, when all Si polymorphs are included in the training-set

5.3 Exploring the limits of two-body potentials

In the previous section, it was shown that it is indeed possible to fit individual two-body repulsive potentials for each and every polymorph that accurately reproduces the corresponding reference DFT data. However, the lack of a one-fits-all solution for the various Si polymorphs clearly demonstrates the problem of transferability associated with repulsive potentials in the SCC-DFTB method. To gain further insight on how to in the end enable the generation of a one-fits-all universal repulsive potential, we analyzed the one- and two-body contributions in more detail for selected pairs of polymorphs.

Let the sets P_{CN1} and P_{CN2} be a class of polymorphs with distinct coordination number (CN). Then, $\forall\ p \in P_{CN1} \cup P_{CN2}$ in a possible one-fits-all procedure can be written as:

$$E^{rep} = \varepsilon_{P_{CN1} \cup P_{CN2}} + V_{P_{CN1} \cup P_{CN2}}(r) \tag{5.1}$$

where ϵ refers to the one-body energy term, and V refers to the two-body potential. Next, we can write the individual fits as:

$$E^{rep} = \varepsilon_{P_{CN1}} + \varepsilon_{P_{CN2}} + V_{P_{CN1}}(r) + V_{P_{CN2}}(r). \tag{5.2}$$

The remaining combination of ϵ's and V's can be written as :

$$E^{rep} = \varepsilon_{P_{CN1}} + \varepsilon_{P_{CN2}} + V_{P_{CN1} \cup P_{CN2}}(r) \tag{5.3}$$

$$E^{rep} = \varepsilon_{P_{CN1} \cup P_{CN2}} + V_{P_{CN1}}(r) + V_{P_{CN2}}(r). \tag{5.4}$$

The above equations were used to study the following combinations: $P_{diamond} \cup P_{SC}$, $P_{SC} \cup P_{BCC}$, $P_{graphene} \cup P_{diamond}$. The results are shown in Fig. 5.3 and show that a simple two-body potential can not even describe a pair of polymorphs simultaneously. Adding multiple ϵ's (one-body terms) improve the overall quality of the fit, albeit only by a small amount. The above analysis indicates that the use of a simple two-body repulsive potential limits the transferability of SCC-DFTB, and to make improvements, many-body characteristics should be included in the repulsive potential.

5.4 Many-body effects in repulsive potentials for SCC-DFTB

As a possible solution to the problem demonstrated in the previous section, the possibility to use Behler-Parinello Neural Networks (BPNN)[72] as repulsive potentials in SCC-DFTB has been investigated. The BPNN

networks are many body neural networks that consider explicit two-body and three-body effects via radial and angular symmetry functions. In **Paper III**, it is shown that a minimal BPNN architecture, with only 2 nodes and 2 hidden layers and a small 4 Å cut-off, is sufficient to accurately reproduce the E-V curves for all Si polymorphs in the training-set (see Fig. 5.4).

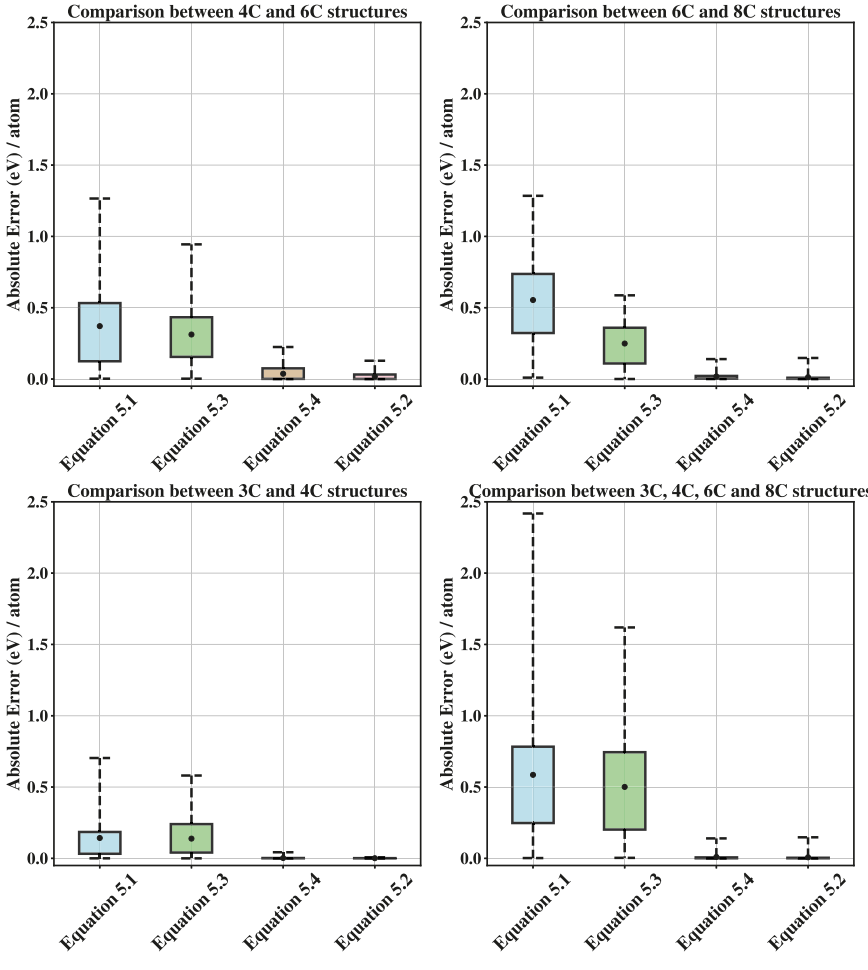

Figure 5.3. The boxplots depict the variation of absolute-errors (y-axis) in the training-set with respect to different models (x-axis) presented in section 5.3. The black dot indicates the mean absolute error, and the whiskers of the boxplot indicate the minimum error and maximum error.

It stands clear that the BPNN approach, owing to the inclusion of many-body effects, is superior to the CCS method when it comes to the accuracy of a one-fits-all general repulsive potential. However, for sparse

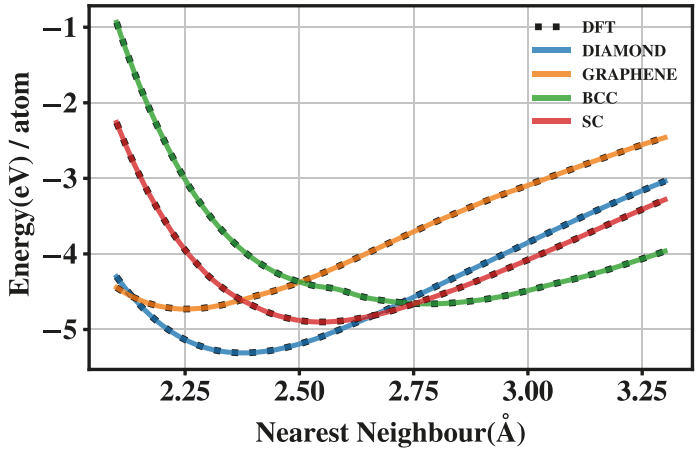

Figure 5.4. Comparison between DFT and SCC-DFTB computed E-V curves for different Si polymorphs using the BPNN one-fits-all general repulsive potential.

data sets, the BPNN approach can result in overfitting. This would not happen using the CCS method owing to the built-in constraints. Thus, the use of BPNN potentials, or other similar formulations, might be problematic for structures that are quite different from the ones included in the training-set. Presently, the only way to ensure the reliability of a BPNN repulsive potential is to train on a vast amount of data. This becomes, however, infeasible when the system contains many different chemical species. In cases where limited transferability is not a significant concern, simple two-body potentials using the CCS methodology would be a better alternative.

6. Paper IV:Electronic properties of correlated electronic states in reduced ceria from SCC-DFTB+U calculations

Purposes:
- To develop an “f in-core" scheme, where Ce $4f$ states are moved into the core, to improve the convergence of the SCC-DFTB+U method.
- Use CCS to have consistent and homogenized repulsive potentials for both explicit and implicit f-electron descriptions.

Methods: DFT, SCC-DFTB, and CCS
Calculated properties: Lattice parameters, the relative stability of vacancies, and electronic properties.
Take-home message: Problems in SCC-DFTB for treating strongly correlated electronic states could be circumvented through the use of a "f in-core" scheme. This was achieved by developing a consistent and harmonized set of SK-tables with corresponding repulsive potentials parameterized using CCS. The developed scheme was able to qualitatively capture the trends as seen in PBE+U, and in the future, might aid exploration of structure-activity relationships in large redox-active nanoparticles.

6.1 Motivation

Reducible metal oxides with strongly correlated d and f electrons are often challenging to study with semi-local DFT. This is due to the self-interaction error (SIE) present in the commonly used DFT functionals[24,73]. We often resort to computationally expensive hybrid functionals or extensions like DFT+U to treat the SIE. So, within the scope of DFT, our understanding is limited to systems of smaller sizes and for shorter timescales. To give some perspective, in chapter 4 section 4.3.2, we studied the relative stability of tetrahedral and octahedral nanoparticles (up to 800 formula units of CeO_2) as a function of size using the CCS+Q method (see Fig. 4.5). It would be nearly impossible to reproduce Fig. 4.5 using DFT. So, we need computationally less demanding alternatives

to DFT to compute electronic structure, and SCC-DFTB is one popular alternative.

The SCC-DFTB method, derived from DFT, inherits many drawbacks from the parent DFT method. Systems with strongly correlated d and f electrons are overdelocalized due to the SIE, which leads to incorrect electronic structure description. An extension similar to DFT+U was derived for SCC-DFTB by Hourahine *et al.*[74] to treat strongly correlated electronic states, and this method, SCC-DFTB+U, has earlier been shown to give a qualitatively good description for various forms of reduced ceria[28]. However, using the SK parameterization developed in Ref.[28] for large systems, with many electronic states leads to problems with the convergence of the SCC cycle. It has been identified that the Ce $4f$ states in CeO_2 are one reason for these convergence problems. This limits large scale simulations for strongly correlated materials using SCC-DFTB.

In **Paper IV**, we suggest a possible solution to this problem using an "f in-core" approach. The method has two clear benefits: *i)* it minimises the convergence issues in SCC-DFTB when dealing with strongly correlated electrons, and *ii)* aids the identification of defect localization patterns in reducible oxides.

6.2 The "f in-core" approach in a nutshell

The key idea behind the "f in-core" approach is to have a consistent (and harmonized) description to switch on and off the Ce $4f$ states. The Ce $4f$ states are moved to the core for an implicit (off) description, while for an explicit (on) description, the Ce $4f$ states are treated as part of the valence. The implicit and explicit description of Ce $4f$ states needs to be harmonized such that we can have both kinds of treatment for Ce $4f$ states concurrently within the same system. This consistency between implicit and explicit description was achieved with repulsive potentials parameterized using the CCS methodology. As an initial test to validate our "f in-core" approach, we apply it to CeO_2 as an example.

Table 6.1. *Connection table for SK-tables.*

	O	Ce	$Ce^{3+}_{fin-core}$	$Ce^{4+}_{fin-core}$
O	mio-1.0[25]	Ref.[28]	x	x
Ce	Ref.[28]	Ref.[28]	x	x
$Ce^{3+}_{fin-core}$	x	x	x	x
$Ce^{4+}_{fin-core}$	x	x	x	x

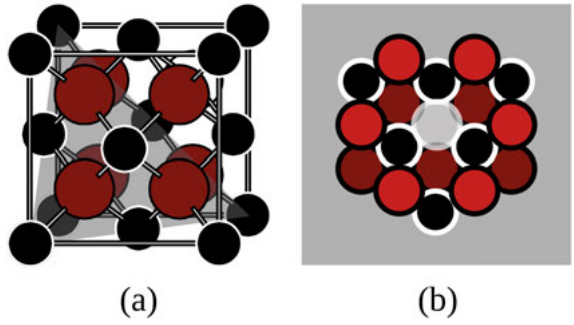

Figure 6.1. a) An illustrative representation of the bulk CeO_2 unit cell. b) The local surrounding of an oxygen vacancy is viewed along the [111] direction. The red circles are oxygen, and the black circles are cerium.

In **Paper IV**, we have developed 12 new sets of SK tables as shown in Table 6.1, apart from the already existing ones from Ref. [28], to account for the two possible charge states of Ce ions in partially reduced ceria. The new ones generated are marked by "x" in the table. The steps involved to generate the SK tables can be summarized as follows: Firstly, we optimized the electronic parameters of the new SK table with Ce $4f$ states in-core towards the electronic structure of the bulk CeO_2 (see Fig. 6.1a). We get a good description for the density of states (DOS) using an SK table with $4f$ states in-core compared to the reference PBE+U data (see Fig. 6.2). Secondly, we turned to partially reduced ceria systems to tune the Hubbard U parameter such that the occupied f-state position relative to the bulk ceria valence band edge matches to that of PBE+U data. For this purpose, we used bulk ceria with oxygen vacancies and a nearest-neighbor (NN) and next-nearest-neighbour (NNN) localization of the existing Ce^{3+} ions. The NN and NNN configurations correspond to having the two Ce^{3+} associated with vacancy located at the inner triangle (NN) or outer triangle (NNN) on Fig. 6.1b. The optimal U-value to reproduce the PBE+U data for the Ce $4f$ occupied state was 1.99 eV. The intention of the above procedure is to ensure that we get the correct description of the localized f electron states when occupied. Lastly, we used the CCS methodology to optimize the respective repulsive potentials to make sure that we got the correct relative energies and structural properties.

The optimization of the repulsive potential plays a crucial part in harmonizing the SK tables, i.e., allows us to use them interchangeably in a system. We have to ensure that both explicit and implicit treatment of Ce $4f$ states gives rise to similar structural properties and relative energies. A more detailed description of the repulsive parametrization can be found in **Paper IV**.

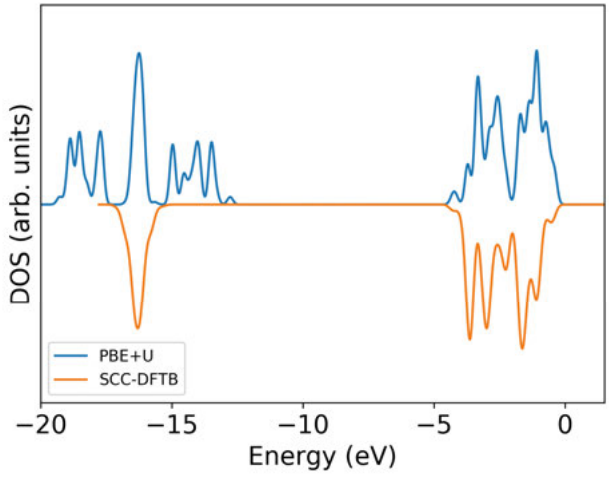

Figure 6.2. Comparison of the DOS computed using PBE+U (U = 5 eV) and SCC-DFTB+U (f in-core) for bulk CeO_2.

6.3 Can the SK tables be used interchangeably?

Table 6.2 summarizes the various settings used for harmonization tests. We either used a approach where the $4f$ states are in-core for all Ce atoms, or a mixed approach where all Ce^{4+} were treated with $4f$ states in-core, and the $4f$ states for expected charge localization centers explicitly treated as valence. The harmonization tests were conducted on V_{NN} and V_{NNN} bulk oxygen vacancies. The results are given in Table 6.3. We qualitatively predicted the correct relative stabilities for V_{NN} and V_{NNN} when compared PBE+U data for all the different harmonization tests. We also got a good agreement for the O $2p$ - Ce $4f$ band gaps. However, the relative energies are all slightly overestimated, but overall we concluded that the SK tables were indeed harmonized and could be used interchangeably.

Table 6.2. *The different settings for harmonization tests.*

	Description
i)	single point with the f in-core potential
ii)	single point using the mixed approach
iii)	full geometry optimization using f in-core
iv)	single point from f in-core optimisation (iii) with the mixed approach
v)	full optimization with the mixed approach

Table 6.3. *Results from the harmonization tests i-v (see. table 6.2). We used a U-value of 1.99 eV for SCC-DFTB+U calculations, and all energies are in eV.*

	$\Delta E(V_{NN} - V_{NNN})$	$E_{gap}^{O_{2p} \rightarrow Ce_{4f}^{occ}}(NN)$	$E_{gap}^{O_{2p} \rightarrow Ce_{4f}^{occ}}(NNN)$
PBE+U	0.07	1.22	1.29
i)	0.15	-	-
ii)	0.12	1.19	1.31
iii)	0.20	-	-
iv)	0.19	1.19	1.24
v)	0.18	1.23	1.20

6.4 Transferability

Are the harmonized SK tables with CCS repulsive potentials transferable to also be used for oxygen vacancies on CeO_2 surfaces? We know from **Paper III** that two-body repulsive potentials in DFTB often have a limited transferability. How transferable is the "f in-core" approach to other CeO_2 systems given that the harmonization depends on the repulsive potential? To address the above questions, we tested the transferability of the "f in-core" approach to study oxygen vacancies on the (111) and (110) CeO_2 surfaces. The stability pattern of the oxygen vacancies on (111) and (110) CeO_2 surfaces are known from the literature[75–77]. For the (111) surface, sub-surface oxygen vacancies (SSV) are more stable as compared to surface vacancies (SV), and electron localization is preferred on the NNN Ce ions (see Fig. 6.3). Similarly, for the (110) surface, NNN Ce^{3+} localization is preferred (see Fig. 6.4). We studied the relative stability of oxygen vacancy formation in the NN and NNN configurations for the CeO_2 (111) and (110) surfaces. We employed three tests: a full geometry optimization with the f in-core approach, a single point (SP) calculation using the mixed approach, and a full relaxation using the mixed approach. We remark that these tests are equivalent to those described in Table 6.3 (see rows ii, iii, and v). The results are given in Table 6.4 and 6.5.

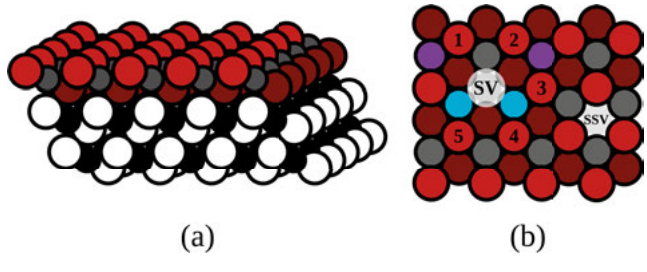

Figure 6.3. a) A schematic representation of a (111) surface slab of CeO_2 (side view). b) Top-view with a surface vacancy (SV) and sub-surface vacancy (SSV). The numbers in b) indicate special oxygen ions surrounding the SV. The turquoise and purple color depicts precise location of Ce^{3+} in the NN and NNN configuration, respectively. Legend is the same as in Fig. 6.1.

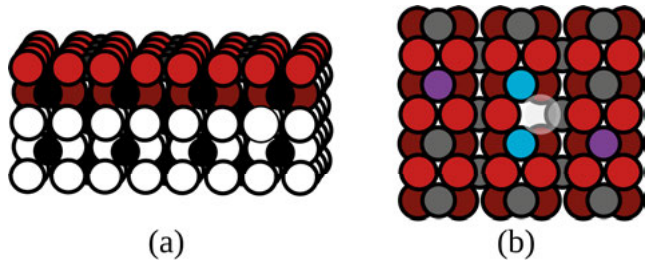

Figure 6.4. a) A schematic representation of a (110) surface slab of CeO_2 (side view). b) Top-view with a surface vacancy (SV) and sub-surface vacancy (SSV). The turquoise and purple color depicts precise location of Ce^{3+} in the NN and NNN configuration, respectively. Legend is the same as in Fig. 6.1.

Table 6.4. *The table shows the relative formation energies in eV for defect formation in bulk ceria and ceria low-index surfaces. The DFTB results are labeled according to Table 6.2. The bulk data for the PBE+U (U = 5 eV) and HSE06 were obtained from Ref. 78. The surface data for PBE+U and HSE06 are taken from Refs. 28 and 79 .*

ΔE	f in-core	mixed (SP)	mixed	PBE+U	HSE06(15%)
bulk V_{NN} - V_{NNN}	0.20	0.19	0.18	0.07	0.10
(111) SSV_{NN}-SSV_{NNN}	0.35	0.68	0.71	0.31	0.44
(111) SV_{NNN}-SSV_{NNN}	0.25	0.38	0.40	0.22	0.18
(111) SV_{NN}-SSV_{NNN}	0.61	0.50	0.54	0.46	0.48
(110) SV_{NN}- SV_{NNN}	0.08	-0.10	-0.16	0.38	-

Our results indicate that the "f in-core" approach correctly predicts the most stable electron localization patterns to be of the NNN type for (111) and (110) CeO_2 surfaces. However, the mixed and mixed (SP) calculation —where $4f$ states are in valence for the reduced ion— incorrectly predicted the vacancy to be more stable in a NN configuration for the (110) surface. We remark that unlike the (111) surface, the (110) surface was not included in the training-set used to fit the repulsive potential. Nevertheless, we got qualitatively good agreement for the relative stability of the vacancies for the bulk and (111) surface for the mixed approach. The structural relaxation around the (111) surface oxygen vacancies are also in good agreement with PBE+U for all three approaches (see Table 6.5).

In the paper, it is shown that a qualitatively correct description of the structure and relative stabilities of oxygen vacancies in bulk ceria and at the low-index surfaces using the f in-core approach is obtained. Including an explicit treatment of the Ce $4f$ electrons, as is done in the mixed approach, reduces the energy and structure transferability. However, we haven not yet established the transferability in electronic properties. For this purpose, we computed the electron DOS (see Fig. 6.5) for the most stable vacancies using a single point mixed approach on the f in-core op-

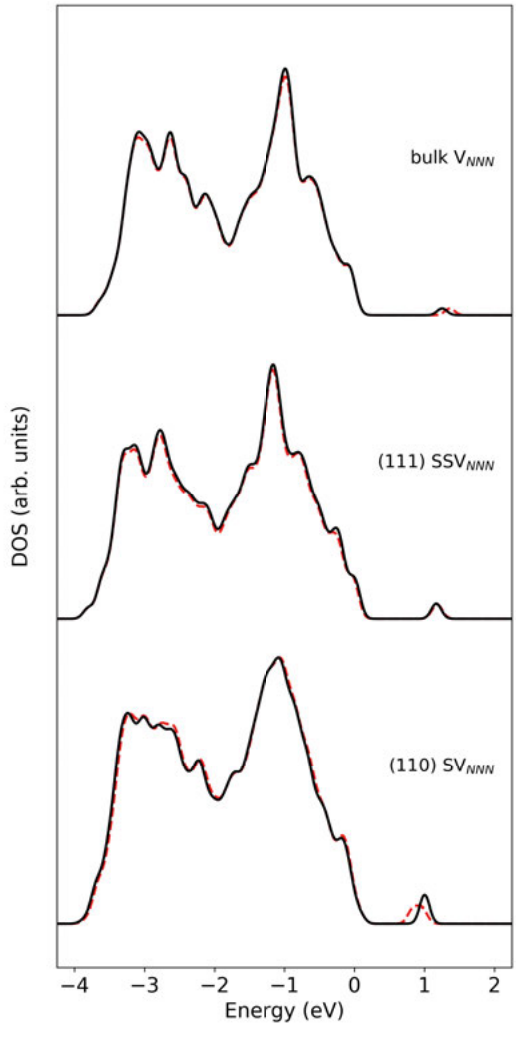

Figure 6.5. Electron DOS for V_{NNN} (top), SSV^{111}_{NNN} (middle) and SV^{110}_{NNN} (bottom). The dashed red lines indicate DOS from mixed(SP) on the "f in-core" optimized structure, and solid black lines indicate DOS from full optimization using the mixed approach.

timized structures, and after a full relaxation using the mixed approach (with an explicit treatment of f electrons). We found that the DOS obtained using both cases were very similar, which implies that the electronic structure is more transferable than the energetic properties. It also implies that the SK tables are completely interchangeable (harmonized) when it comes to this property. In principle, we can substitute geometry

Table 6.5. *O-O distances (in Å) around the (111) surface oxygen vacancy*

Method	f in-core	mixed	PBE+U
	NN		
$r(O_1 - O_2)$	3.81	3.82	3.83
$r(O_2 - O_3)$	3.96	3.95	3.95
$r(O_3 - O_4)$	4.11	4.08	4.14
$r(O_4 - O_5)$	3.97	3.96	3.96
	NNN		
$r(O_1 - O_2)$	3.60	3.59	3.61
$r(O_2 - O_3)$	4.21	4.23	4.25
$r(O_3 - O_4)$	3.69	3.68	3.67
$r(O_4 - O_5)$	3.95	3.97	4.01

optimisation with $4f$ states in valence (mixed approach) by a single point calculation on a structure optimized with an implicit description of the $4f$ states. The latter method provides us a faster alternative to find the position of $4f$ states in relation to the bulk valence band (mainly O $2p$ states), which is particularly useful for large systems with problematic SCC convergence.

7. Future outlook

This thesis primarily focused on the development of the CCS methodology and its application as a tool for linking and coupling in multiscale modelling schemes. The advantage of using the CCS method has been mentioned in this thesis. Here, I discuss about the possible improvements that can be made in future versions of the CCS methodology.

When used in the SCC-DFTB framework, it was found that a two-body repulsive potential is not sufficient to attain transferability and to solve this, a many-body approacy such as the BPNN is needed. Another route along the same direction would be to include a short-ranged three-body contribution which has earlier been shown to improve the accuracy of SCC-DFTB.[66] The three-body energy expression can be written as follows:

$$E^{3-body}(r_i, r_j, r_k) = \sum_{i<j<k} f(r_{ij}, r_{jk}, r_{ik}) \tag{7.1}$$

where $f(r_{ij}, r_{jk}, r_{ik})$ is a three dimensional function and i, j, k run over all atoms in the system. Within the current formalism of the CCS method, such terms could be described by tri-cubic splines or B-splines taking three distances of a triangle of atoms as input. Furthermore, constraints similar to those used in our 2-body expression could be applied also here, but the appropriate form of them would need to be determined. Sparse data could be handled by merging sub-cubes on the 3D spline grid using a similar technique as that presented in section 3.2.2. The advantage of this approach would be that its freed from additional meta-parameters (apart from cut-off radius) and that the method would remain linear in the parameters needed to be determined. A very similar extension was suggested by Goldman *et al.*[66] using Chebyshev polynomials, albeit without the constraints.

The quality of a CCS potential depends on the quality of the training-set used. Like any other ML model, CCS potentials can be poor in regions on the PES where it has not been trained. The constraints reduce this error significantly. Nevertheless, constructing, or, choosing, a good training-set is not a trivial problem. A brute force way out is to perform millions of QM calculations on the PES. This is, however, computationally very expensive and impractical. A more practical solution would be to implement a train on the fly approach.

Active learning based on a D-optimality criterion as proposed by Podryabinkin and Shapeev [80] can be used as a tool to identify configurations on which the ML potential extrapolates. This is applicable to linearly parameterized interatomic potentials like CCS, moment tensor potetntial (MTP) etc. This could be used to reduce the training-set size and provide a better way to construct the training-set for CCS model in the future.

8. Concluding remarks

In 1929, the Nobel laureate and famous quantum physicist Paul Dirac stated:

"The underlying physical laws necessary for the mathematical theory of a large part of physics and the whole of chemistry are thus completely known, and the difficulty is only that the exact application of these laws leads to equations much too complicated to be soluble. It therefore becomes desirable that approximate practical methods of applying quantum mechanics should be developed, which can lead to an explanation of the main features of complex atomic systems without too much computation."

It is clear from the discussions and results presented in this thesis that this quote is as relevant now as when it was stated. Still, approximate QM models and methods are being developed with the aim to overcome the practical difficulties associated with solving the basic QM equations. Today, however, the mathematical models used to approximate the complicated QM relations are becoming almost as complex as the original ones. For example, models that has become popular today are often highly non-linear and with an increasing number of parameters, thereby becoming extremely tedious to parameterise, and tedious to solve. Most often, supercomputer facilities are required since the parameterisation relies on resource-hungry heuristic and meta-heuristic algorithms.

The main result of this thesis is the development of the CCS methodology (**Paper I**), which uses linear models to improve the quality and parametrisation processes of two-body potentials for linking between and within electronic and atomistic levels in Fig. 1.1. As such, an alternative route to the computer extensive data driven approaches is provided with the intention to be more computationally effective by the use of simple interaction models, both in terms mathematical form and when it comes to the parameterization process.

The CCS model is linear, which implies that parameters can be easily solved in a least-square sense using a QP approach. Moreover, the objective function is convex, which ensures that any found minimum is a global minimum. This makes the optimisation process easy to handle and requires little to no human effort. Initial tests to validate the method were performed on molecular and bulk neon structures. In **Paper II**, the CCS methodology was extended to also incorporate long-range interactions by including atomic charges. Within the same philosophy,

also the magnitude of the atomic charges (Q) could be optimised in a linear fashion simultaneously with the other CCS parameters, making the whole process of fitting combined long-range and short-range interactions easier. The capabilities of the method, abbreviated CCS+Q, was demonstrated for ZnO polymorphs, and at the same time bench-marked towards use of the conventional approach using Buckingham potentials for the same problem. The results indicate that the CCS+Q method performs on par with the Buckingham approach, but is much faster and easier to parameterise. The method is further demonstrated for a more chemically diverse problem, size dependent shapes of CeO_2 nanoparticles.

The CCS method was further employed to develop repulsive potentials in SCC-DFTB (**Paper III**). The parametrisation of the two-body repulsive potentials is the major bottleneck in development of SCC-DFTB parameters. The use of CCS made this process simpler, and further provided new opportunities to explore the limits of the SCC-DFTB method. The results suggest that the repulsive potentials should have many-body characteristics to achieve transferability, which was corroborated by the many body BPNN based repulsive potentials for Si polymorphs. The versatile CCS method was used to develop interchangeable Slater-Koster tables for Ce ions of various oxidation states, referred to as the harmonization process, thus improving the scalability of the SCC-DFTB simulations for highly correlated electron systems (**Paper IV**).

In summary, this thesis highlights the importance, usefulness, and applicability of linear models to solve some of the existing problems in computational material science.

9. Acknowledgement

I would like to sincerely thank my supervisors Dr. Peter Broqvist, Dr. Jolla Kullgren, and Dr. Eddie Wadbro, for their guidance and support throughout my studies. Peter, you have taught me to look at the scientific problems from a broader perspective, allowed me to pursue my strengths and research interests, and has always been an ideal mentor. Jolla, your ideas form the foundation of my thesis. Your pragmatic approach and clarity of thought have always been a great source of inspiration. Eddie, you have always cleared my doubts without exception. Thank you for having the patience to explain things with such clarity.

I want to thank Prof. Kersti Hermansson for all the scientific and non-scientific discussions. Kersti, you have always ensured that I felt comfortable in Uppsala. Thank you for all the support and guidance you have provided me.

I want to take this opportunity to thank all the former and current members of the TEOROO/CMC family for all their help and support. Ageo, thank you for having my back in dire situations. Simon, thank you for helping me with the popular scientific summary in swedish. Pavlin, thank you for all the help with AWK and linux. Esteban, thank you for all the help with Mathematica.

I thank the financial support from Swedish Research Council (VR), the Center for Interdisciplinary Mathematics (CIM), and the Swedish National Strategic e-Science programme (eSSENCE). I also thank the Swedish National Infrastructure for Computing(SNIC) at UPPMAX and NSC for providing computational resources.

I thank the unconditional support from my wife Athira and parents. Last but not least, I thank my friends (Jithin, Geethu, Vishnu, Anu, Alma, Athira, Harish, and IISER batchmates) for making my stay in Sweden memorable.

10. Swedish summary

Avancerade material har revolutionerat vår vardag. Apparater som pekskärmstelefoner och eldrivna fordon har blivit centrala i vårt samhälle. Dessa tekniska bedrifter möjliggjordes av de fascinerande egenskaperna, på olika längdskalor, hos avancerade material. Till exempel är egenskaperna hos kopparnanopartiklar (ett material som är mindre än 50 nm) mycket olika från bulkkoppars egenskaper. Bulkkoppar används i ledande kablar på grund av sin mjukhet. I kontrast formar kopparnanopartiklar ett mycket hårt material. Ända sedan forskare observerade dessa egenskaper har de brottats med frågan: Varför ändras egenskaper hos ett material med storlek och form? Richard Feynman sa i sina föreläsningar om fysik att mycket av världen skulle kunna förstås med atomhypotesen: ”att alla saker är gjorda av atomer — små partiklar som rör sig i eviga rörelser, dessa attraherar varandra när de befinner sig på ett litet avstånd från varandra, men är repulsiva när de pressas in i varandra”. Han föreslår att ”med bara lite fantasi och tänkande” skulle man kunna berätta enormt mycket om världen. Faktum är att hans argument är korrekta och disciplinen ”Materialvetenskap” handlar om att identifiera och förstå förhållandet mellan materialets struktur och dess egenskaper. Men hur bestämmer vi strukturen hos ett material som är osynligt för blotta ögat?

Nyligen skedde ett stort genombrott inom materialvetenskap, för första gången uppnåddes supraledning (elektroner som flödar utan friktion) i ett material vid rumstemperatur. Materialet bestod av kol, väte och svavel. Supraledning uppnåddes vid temperaturer runt 288 K vid ett tryck på 155GPa – motsvarande 1,55 miljoner gånger trycket från jordens atmosfär. Experimenten som utfördes kunde dock inte identifiera atomernas exakta positioner och datormodeller användes för att ge en gissning av den troliga strukturen. Även om kemi ofta anses vara en experimentell vetenskap krävs ofta teoretiska modeller för att komplettera experimenten. I själva verket tilldelades Nobelpriset 2013 i kemi till Martin Karplus från Harvard University, USA, Michael Levitt från Stanford University, US och Arieh Warshel från University of Southern California, US, för "utveckling av flerskaliga modeller för komplexa kemiska system".

Elektronerna rör sig med mycket hög hastighet i dessa material, och deras rörelse följer kvantmekanikens lagar. I princip kan vi använda dessa lagar och beräkna elektronernas framtida position på penna och papper.

Denna process är dock mycket komplicerad och ibland praktiskt omöjlig, vilket tvingar oss att söka hjälp från datorer. Genom åren har en snabb utveckling inom beräkningsteknik låtit oss bli bättre på modellering av kemi. Men det finns fortfarande flera utmaningar. Till exempel innehåller en mol (måttenhet i kemi) av ett ämne 10^{23} partiklar. Att använda kvantmekaniska metoder för att beskriva så stora system är inte ens möjligt för toppmoderna superdatorer. Emellertid kan atomernas rörelse beskrivas med Newtons ekvationer, vilket är betydligt enklare att beräkna än ekvationerna för elektronerna. En naturlig fråga som uppstår är om elektronernas rörelse är kopplad till atomernas rörelse. I allmänhet kan detta antas vara falskt. Detta beror på att elektroner är mycket lättare än atomer, vilket innebär att de rör sig betydligt snabbare än atomerna. Därför kan vi frånkoppla elektronernas rörelse från atomernas. På liknande sätt kan en serie approximationer göras för att ytterligare minska modellernas komplexitet. Således kan material modelleras i olika längd- och tidsskalor.

Mycket av forskningen på små skalor fokuserar antingen på atomnivå eller elektronnivå. På elektronnivå är modellerna mycket exakta men långsamma och på atomnivå är modellerna snabba men mer osäkra. Helst vill vi ha ett arbetsflöde där vi kan gå från att beskriva elektroner till att beskriva atomer, utan betydande förlust av noggrannhet och samtidigt kunna utföra beräkningen snabbt. För närvarande finns det två klasser av modeller som används för att överföra information mellan elektron- och atombeskrivningarna. Den första klassen av metoder kallas fysikbaserade metoder och den andra klassen av metoder kallas datadrivna metoder. Nyligen har datadrivna metoder vunnit popularitet i beräkningsmaterialvetenskapen. De är mycket noggranna, men en stor brist är att de är kräver en långrandig utvecklingsprocess. En stor mängd data (vanligtvis i miljontals datapunkter) krävs för att konstruera datadrivna modeller. De fysik härledda metoderna kräver mycket mindre data men är mindre korrekta. I **artikel I** utvecklade vi en metod som kallas Curvature Constrained Splines (CCS) som ger en bra kompromiss mellan datadrivna och fysikbaserade modeller. Här testade vi denna modellen på enkla ädelgaser för att göra en prestandajämförelse. Vidare utvidgade vi i **artikel II** CCS-modellen att inkludera kvanteffekter (CCS+Q) för att fånga en större klass av material. Den utökade metoden användes för att studera ZnO och CeO_2. Vi fann att CCS+Q-metoden var bättre än vanligt använda fysikbaserade modeller.

Efter att ha fastställt ramverket för CCS-metoden användes den vidare för att länka två olika elektronmodeller som heter DFT och DFTB i **artikel III**. Parametriseringen av repulsiva potentialer är normalt en långdragen och tidskrävande process. Användningen av CCS gjorde denna process betydligt effektivare och gav ytterligare möjligheter att utforska gränserna för modellen. Utvecklingen av repulsiva potentialer för

Si-polymorfer i bulk visade att det är möjligt att generera en bra beskrivning av varje enskild polymorf, men omöjligt erhålla en samtidig acceptabel beskrivning av alla polymorfer. Vi visar att en överförbar repulsiv potential behöver ha ett koordinationssberoende. Användandet av ett artificiellt neuralt nätverk för att representera den repulsiva potentialen resulterar i en bättre överförbarhet. I **artikel IV** använde vi CCS för att övervinna konvergensproblemen i SCC-DFTB för starkt korrelerade system. Sammanfattningsvis, CCS-metoden visar sig vara ett mångsidigt verktyg för effektiv koppling mellan (och inom) elektroniska och atomistiska modeller

References

[1] R. P. Feynman, R. B. Leighton, and M. Sands, *The Feynman lectures on physics, Vol. I: The new millennium edition: mainly mechanics, radiation, and heat*, Vol. 1 (Basic books, 2011).

[2] S. Auvinen, M. Alatalo, H. Haario, J. P. Jalava, and R. J. Lamminmäki, J. Phys. Chem. C **115**, 8484 (2011).

[3] B. D. Chithrani, A. A. Ghazani, and W. C. Chan, Nano Lett. **6**, 662 (2006).

[4] A. Trovarelli, Catal. Rev. - Sci. Eng. **38**, 439 (1996).

[5] A. S. Aricò, P. Bruce, B. Scrosati, J. M. Tarascon, and W. Van Schalkwijk, Nat. Mater. **4**, 366 (2005).

[6] Z. W. She, J. Kibsgaard, C. F. Dickens, I. Chorkendorff, J. K. Nørskov, and T. F. Jaramillo, "Combining theory and experiment in electrocatalysis: Insights into materials design," (2017).

[7] S. Y. Huang, L. Kavan, I. Exnar, and M. Grätzel, J. Electrochem. Soc. **142**, L142 (1995).

[8] R. Rousseau, V. A. Glezakou, and A. Selloni, Nat. Rev. Mater. **5**, 460 (2020).

[9] A. Trovarelli and P. Fornasiero, *Catalysis by ceria and related materials; 2nd ed.*, Catalytic Science Series (World Scientific, Singapore, 2013).

[10] A. Bruix, J. T. Margraf, M. Andersen, and K. Reuter, Nat. Catal. **2**, 659 (2019).

[11] A. A. Franco, RSC Adv. **3**, 13027 (2013).

[12] A. A. Franco, A. Rucci, D. Brandell, C. Frayret, M. Gaberscek, P. Jankowski, and P. Johansson, Chem. Rev. **119**, 4569 (2019).

[13] N. M. Ghoniem†, E. P. Busso, N. Kioussis, and H. Huang, Philos. Mag. **83**, 3475 (2003).

[14] A. F. de Baas, *What makes a material function? - Publications Office of the EU* (Publications Office of the European Union, 2017).

[15] V. Fock, Zeitschrift für Phys. **61**, 126 (1930).

[16] P. Hohenberg and W. Kohn, Phys. Rev. **136**, B864 (1964).

[17] W. Kohn and L. J. Sham, Phys. Rev. **140**, A1133 (1965).

[18] J. Townsend, J. K. Kirkland, and K. D. Vogiatzis, in *Math. Phys. Theor. Chem.* (Elsevier, 2018) pp. 63–117.

[19] W. Thiel, Wiley Interdiscip. Rev. Comput. Mol. Sci. **4**, 145 (2014).

[20] A. Jain, Y. Shin, and K. A. Persson, Nat. Rev. Mater. **1**, 1 (2016).

[21] A. J. Cohen, P. Mori-Sánchez, and W. Yang, "Challenges for density functional theory," (2012).

[22] K. Burke, J. Chem. Phys. **136**, 150901 (2012), arXiv:1201.3679 .

[23] J. P. Perdew, W. Yang, K. Burke, Z. Yang, E. K. Gross, M. Scheffler, G. E. Scuseria, T. M. Henderson, I. Y. Zhang, A. Ruzsinszky, H. Peng,

J. Sun, E. Trushin, and A. Görling, Proc. Natl. Acad. Sci. U. S. A. **114**, 2801 (2017).
[24] G. Pacchioni, J. Chem. Phys. **128**, 182505 (2008).
[25] M. Elstner, D. Porezag, G. Jungnickel, J. Elsner, M. Haugk, and T. Frauenheim, Phys. Rev. B - Condens. Matter Mater. Phys. **58**, 7260 (1998).
[26] T. Frauenheim, G. Seifert, M. Elstner, Z. Hajnal, G. Jungnickel, D. Porezag, S. Suhai, and R. Scholz, Phys. Status Solidi Basic Res. **217**, 41 (2000).
[27] M. Elstner, Theor. Chem. Acc. **116**, 316 (2006).
[28] J. Kullgren, M. J. Wolf, K. Hermansson, C. Köhler, B. Aradi, T. Frauenheim, and P. Broqvist, J. Phys. Chem. C **121**, 4593 (2017).
[29] E. Erdogan, I. H. Popov, A. N. Enyashin, and G. Seifert, Eur. Phys. J. B **85**, 33 (2012).
[30] R. G. Parr, in *Horizons Quantum Chem.* (Springer Netherlands, 1980) pp. 5–15.
[31] W. Koch and M. C. Holthausen, *A Chem. Guid. to Density Funct. Theory* (Wiley, 2001).
[32] J. P. Perdew and K. Schmidt, AIP Conf. Proc. **577**, 1 (2001).
[33] G. Kresse and J. Hafner, Phys. Rev. B **47**, 558 (1993).
[34] G. Kresse and J. Hafner, Phys. Rev. B **49**, 14251 (1994).
[35] G. Kresse and J. Furthmüller, Comput. Mater. Sci. **6**, 15 (1996).
[36] G. Kresse and J. Furthmüller, Phys. Rev. B - Condens. Matter Mater. Phys. **54**, 11169 (1996).
[37] P. Koskinen and V. Mäkinen, Comput. Mater. Sci. **47**, 237 (2009), arXiv:arXiv:0910.5861v1 .
[38] B. Aradi, B. Hourahine, and T. Frauenheim, J. Phys. Chem. A **111**, 5678 (2007).
[39] B. Hourahine, B. Aradi, V. Blum, F. Bonafé, A. Buccheri, C. Camacho, C. Cevallos, M. Y. Deshaye, T. Dumitric, A. Dominguez, S. Ehlert, M. Elstner, T. Van Der Heide, J. Hermann, S. Irle, J. J. Kranz, C. Köhler, T. Kowalczyk, T. Kubař, I. S. Lee, V. Lutsker, R. J. Maurer, S. K. Min, I. Mitchell, C. Negre, T. A. Niehaus, A. M. Niklasson, A. J. Page, A. Pecchia, G. Penazzi, M. P. Persson, J. Å&tild;ezáč, C. G. Sánchez, M. Sternberg, M. Stöhr, F. Stuckenberg, A. Tkatchenko, V. W. Yu, and T. Frauenheim, J. Chem. Phys. **152**, 124101 (2020).
[40] M. S. Daw and M. I. Baskes, Phys. Rev. B **29**, 6443 (1984).
[41] J. Tersoff, Phys. Rev. B **37**, 6991 (1988).
[42] J. Behler, J. Chem. Phys. **145**, 170901 (2016).
[43] T. Mueller, A. Hernandez, and C. Wang, "Machine learning for interatomic potential models," (2020).
[44] S. Vavasis (1998).
[45] S. Diamond and S. Boyd, J. Mach. Learn. Res. **17**, 1 (2016), arXiv:1603.00943 .
[46] M. Gaus, C. P. Chou, H. Witek, and M. Elstner, J. Phys. Chem. A **113**, 11866 (2009).

[47] A. Mondal, J. M. Young, T. A. Barckholtz, G. Kiss, L. Koziol, and A. Z. Panagiotopoulos, J. Chem. Theory Comput. **16**, 5736 (2020).
[48] G. L. Rech, A. L. Martinotto, N. M. Balzaretti, and C. A. Perottoni, Comput. Mater. Sci. **187**, 109929 (2021).
[49] M. Matsui and M. Akaogi, Mol. Simul. **6**, 239 (1991).
[50] B. Luan, T. Huynh, and R. Zhou, J. Chem. Phys. **142**, 234102 (2015).
[51] S. Wang, Z. Fan, R. S. Koster, C. Fang, M. A. Van Huis, A. O. Yalcin, F. D. Tichelaar, H. W. Zandbergen, and T. J. H. Vlugt, (2014), 10.1021/jp411308z.
[52] J. D. Gale, Philos. Mag. B Phys. Condens. Matter; Stat. Mech. Electron. Opt. Magn. Prop. **73**, 3 (1996).
[53] C. R. Catlow, C. M. Freeman, M. S. Islam, R. A. Jackson, M. Leslie, and S. M. Tomlinson, Philos. Mag. A Phys. Condens. Matter, Struct. Defects Mech. Prop. **58**, 123 (1988).
[54] R. S. Mulliken, J. Chem. Phys. **23**, 1833 (1955).
[55] P. O. Löwdin, J. Chem. Phys. **18**, 365 (1950).
[56] F. L. Hirshfeld, Theor. Chim. Acta **44**, 129 (1977).
[57] F. A. Momany, J. Phys. Chem. **82**, 592 (1978).
[58] S. R. Cox and D. E. Williams, J. Comput. Chem. **2**, 304 (1981).
[59] T. A. Manz and D. S. Sholl, J. Chem. Theory Comput. **6**, 2455 (2010).
[60] P. P. Ewald, Ann. Phys. **369**, 253 (1921).
[61] A. Migani, K. M. Neyman, and S. T. Bromley, Chem. Commun. **48**, 4199 (2012).
[62] J. M. Knaup, B. Hourahine, and T. Frauenheim, J. Phys. Chem. A **111**, 5637 (2007).
[63] Z. Bodrog, B. Aradi, and T. Frauenheim, J. Chem. Theory Comput. **7**, 2654 (2011).
[64] M. Doemer, E. Liberatore, J. M. Knaup, I. Tavernelli, and U. Rothlisberger, Mol. Phys. **111**, 3595 (2013).
[65] M. Hellström, K. Jorner, M. Bryngelsson, S. E. Huber, J. Kullgren, T. Frauenheim, and P. Broqvist, J. Phys. Chem. C **117**, 17004 (2013).
[66] N. Goldman, L. E. Fried, and L. Koziol, J. Chem. Theory Comput. **11**, 4530 (2015).
[67] C. Panosetti, A. Engelmann, L. Nemec, K. Reuter, and J. T. Margraf, J. Chem. Theory Comput. **16**, 2181 (2020).
[68] M. Stöhr, L. Medrano Sandonas, A. Tkatchenko, L. M. Sandonas, A. Tkatchenko, L. Medrano Sandonas, and A. Tkatchenko, J. Phys. Chem. Lett. **11**, 6835 (2020), arXiv:2006.10429 .
[69] S. Markov, G. Penazzi, Y. Kwok, A. Pecchia, B. Aradi, T. Frauenheim, and G. Chen, IEEE Electron Device Lett. **36**, 1076 (2015).
[70] S. Markov, B. Aradi, C. Y. Yam, H. Xie, T. Frauenheim, and G. Chen, IEEE Trans. Electron Devices **62**, 696 (2015).
[71] C. P. Chou, Y. Nishimura, C. C. Fan, G. Mazur, S. Irle, and H. A. Witek, J. Chem. Theory Comput. **12**, 53 (2016).
[72] J. Behler and M. Parrinello, Phys. Rev. Lett. **98**, 146401 (2007).
[73] V. I. Anisimov, J. Zaanen, and O. K. Andersen, Phys. Rev. B **44**, 943 (1991).

[74] B. Hourahine, S. Sanna, B. Aradi, C. Köhler, T. Niehaus, and T. Frauenheim, in *J. Phys. Chem. A*, Vol. 111 (2007) pp. 5671–5677.
[75] M. Nolan, S. Grigoleit, D. C. Sayle, S. C. Parker, and G. W. Watson, Surf. Sci. **576**, 217 (2005).
[76] M. Nolan, J. E. Fearon, and G. W. Watson, Solid State Ionics **177**, 3069 (2006).
[77] M. V. Ganduglia-Pirovano, J. L. Da Silva, and J. Sauer, Phys. Rev. Lett. **102**, 026101 (2009).
[78] D. Du, M. J. Wolf, K. Hermansson, and P. Broqvist, Phys. Rev. B **97**, 235203 (2018).
[79] J. Paier, C. Penschke, and J. Sauer, Chemical reviews **113**, 3949 (2013).
[80] E. V. Podryabinkin and A. V. Shapeev, Comput. Mater. Sci. **140**, 171 (2017), arXiv:1611.09346 .

Acta Universitatis Upsaliensis

Digital Comprehensive Summaries of Uppsala Dissertations from the Faculty of Science and Technology 2017

Editor: The Dean of the Faculty of Science and Technology

A doctoral dissertation from the Faculty of Science and Technology, Uppsala University, is usually a summary of a number of papers. A few copies of the complete dissertation are kept at major Swedish research libraries, while the summary alone is distributed internationally through the series Digital Comprehensive Summaries of Uppsala Dissertations from the Faculty of Science and Technology. (Prior to January, 2005, the series was published under the title "Comprehensive Summaries of Uppsala Dissertations from the Faculty of Science and Technology".)

Distribution: publications.uu.se
urn:nbn:se:uu:diva-434283

ACTA
UNIVERSITATIS
UPSALIENSIS
UPPSALA
2021